

**Implementation of a Total Power Radiometer in Software Defined Radios**

by

Matthew Erik Nelson

A thesis submitted to the graduate faculty  
in partial fulfillment of the requirements for the degree of  
**MASTER OF SCIENCE**

Major: Computer Engineering (Embedded Systems)

Program of Study Committee:

Phillip H Jones, Major Professor

John Basart

Brian K. Hornbuckle

Iowa State University

Ames, Iowa

2015

Copyright © Matthew Erik Nelson, 2015. All rights reserved.

## **DEDICATION**

I would like to dedicate this thesis to my wife Jennifer who has stood by me through this long journey towards my Masters. She put up with my countless afternoons that I was gone working on my thesis and also helped edit my thesis.

I would also like to thank my parents without whose support I would not have been able to complete this work.

I would also like to thank my friends and family for their continued support and constant encouragement.

**TABLE OF CONTENTS**

<b>LIST OF TABLES . . . . .</b>	<b>vi</b>
<b>LIST OF FIGURES . . . . .</b>	<b>vii</b>
<b>ACKNOWLEDGEMENTS . . . . .</b>	<b>xi</b>
<b>CHAPTER 1. INTRODUCTION . . . . .</b>	<b>1</b>
<b>CHAPTER 2. RELATED WORKS . . . . .</b>	<b>4</b>
2.1 Digital Radiometers . . . . .	4
2.2 Software Defined Radio Based Radiometers . . . . .	5
2.3 Radio Frequency Interference (RFI) Mitigation . . . . .	6
<b>CHAPTER 3. BACKGROUND . . . . .</b>	<b>8</b>
3.1 Radiometer Basics . . . . .	8
3.1.1 Power Measurement . . . . .	9
3.1.2 Radiometer Performance Metrics . . . . .	11
3.2 Software Defined Radios Basics . . . . .	15
3.3 Software Defined Radio Development Platform . . . . .	16
3.3.1 Hardware Platform . . . . .	17
3.3.2 Software Platform . . . . .	19
<b>CHAPTER 4. SOFTWARE DEFINED RADIOMETER IMPLEMENTATION . . . . .</b>	<b>22</b>
4.1 Requirements . . . . .	22
4.2 Mapping Traditional Radiometer Functions to a Software Defined Radio Based Radiometer . . . . .	23

4.2.1	Power measurement . . . . .	23
4.2.2	Data filtering . . . . .	25
4.2.3	Bandwidth limitation . . . . .	27
4.3	Software Defined Radio Based Radiometer Control System . . . . .	28
4.3.1	Control of the SDR based radiometer through GNURadio . . . . .	28
4.3.2	Impact of the Controls Related to Radiometry . . . . .	29
4.3.3	GNURadio Data Display . . . . .	29
<b>CHAPTER 5. EVALUATION SETUP AND EXPERIMENTAL DESIGN . . . . .</b>		34
5.1	Experiment I - Software Defined Radiometer Verification and Calibration . . . . .	34
5.1.1	Experimental setup . . . . .	35
5.1.2	Data Collection . . . . .	37
5.2	Experiment II - Verification of sensitivity and stability . . . . .	39
5.2.1	Experimental setup . . . . .	40
5.2.2	Data Collection . . . . .	40
5.3	Experiment III - Interfering Signal Mitigation . . . . .	40
5.3.1	Experimental setup . . . . .	41
5.3.2	Data Collection . . . . .	42
5.4	Experiment IV - Performance impact of interfering signal mitigation . . . . .	42
5.4.1	Experimental setup . . . . .	43
5.4.2	Data Collection . . . . .	43
<b>CHAPTER 6. RESULTS AND ANALYSIS . . . . .</b>		44
6.1	Experiment I - Software Defined Radio Based Radiometer Verification and Calibration . . . . .	44
6.1.1	Data Collected . . . . .	44
6.1.2	Data Analysis . . . . .	45
6.2	Experiment II - Evaluation of sensitivity and stability . . . . .	48
6.2.1	Data Collected . . . . .	48
6.2.2	Data Analysis . . . . .	49

6.3	Experiment III - Interfering Signal Mitigation . . . . .	51
6.3.1	Data Collected . . . . .	52
6.3.2	Data Analysis . . . . .	52
6.4	Experiment IV - Performance impact of interfering signal mitigation . . . . .	55
6.4.1	Data Collected . . . . .	56
6.4.2	Data Analysis . . . . .	56
6.4.3	Usage Scenario . . . . .	59
6.5	Advantages of a Software Defined Radio Based Radiometer . . . . .	62
6.5.1	Cost Benefits . . . . .	63
6.5.2	Weight and component size benefits . . . . .	65
6.5.3	Value added benefits . . . . .	66
6.6	Drawbacks of a SDR-based Radiometer . . . . .	67
6.6.1	Power Consumption . . . . .	68
6.6.2	Bandwidth constraints . . . . .	68
<b>CHAPTER 7.</b>	<b>CONCLUSION AND FUTURE WORK . . . . .</b>	<b>70</b>
7.1	Conclusion . . . . .	70
7.2	Future work . . . . .	70
7.2.1	Improvements . . . . .	70
7.2.2	Further testing . . . . .	73
7.3	Closing statement . . . . .	73
<b>APPENDIX A.</b>	<b>Source code . . . . .</b>	<b>74</b>
<b>BIBLIOGRAPHY . . . . .</b>		<b>89</b>

**LIST OF TABLES**

Table 4.1	Required Radiometer performance . . . . .	23
Table 6.1	Total Power calibration data points . . . . .	44
Table 6.2	Total Power calibration data points for the stability experiment . . . . .	49
Table 6.3	Experimental parameters for experiment one. . . . .	49
Table 6.4	Total Power calibration data points . . . . .	52
Table 6.5	Measured sensitivity and Bandwidth of Filter . . . . .	62
Table 6.6	Measured Total Power and Bandwidth of Signal . . . . .	63
Table 6.7	Cost Analysis . . . . .	64
Table 6.8	Weight Analysis . . . . .	68

## LIST OF FIGURES

Figure 3.1	A total power radiometer block diagram . . . . .	9
Figure 3.2	A block diagram of a Dicke radiometer . . . . .	13
Figure 3.3	A block diagram of a Noise Injection radiometer . . . . .	14
Figure 3.4	An ideal software defined radio . . . . .	15
Figure 3.5	A typical software defined radio . . . . .	16
Figure 3.6	The USRP N200 from Ettus Research (Image from Ettus Research Website - <a href="http://www.ettus.com">www.ettus.com</a> ) . . . . .	17
Figure 3.7	A block diagram of the Ettus N200 SDR. (Image from Ettus Research Website - <a href="http://www.ettus.com">www.ettus.com</a> ) . . . . .	18
Figure 3.8	The DBSRX2 daughter board from Ettus Research (Image from Ettus Research Website - <a href="http://www.ettus.com">www.ettus.com</a> ) . . . . .	19
Figure 3.9	Block diagram of the DBSRX2 daughter board. . . . .	20
Figure 3.10	A screenshot of the GNURadio Companion editor program. Source: GNURadio . . . . .	21
Figure 4.1	A simple diagram of a square-law detector. . . . .	24
Figure 4.2	A block diagram of the power detection, low pass filter and decimation block used for total power measurements. . . . .	24
Figure 4.3	Power measurements from a square law detector before filtering . . . . .	25
Figure 4.4	A simple RC circuit. . . . .	26
Figure 4.5	Power measurements from a square law detector after filtering . . . . .	27
Figure 4.6	Impulse input and the response of a RC low pass filter . . . . .	30
Figure 4.7	Impulse input and the response of a RC low pass filter . . . . .	31

Figure 4.8	A screenshot of the interface made for communication with and controlling the software defined radio . . . . .	32
Figure 4.9	A screenshot showing the ticker tape display for the total power readings. In addition, raw and calibrated noise temperature is shown below.	33
Figure 5.1	Block diagram of Experiment 1 setup. Source: Matthew E. Nelson . .	35
Figure 5.2	The radiometer RF front end with LNAs and band-pass filters used in the experiments. Source: Matthew E. Nelson . . . . .	36
Figure 5.3	The File Sink block used in GNURadio. Source: GNURadio . . . . .	37
Figure 5.4	The ADL50902 IC on a demonstration board. . . . .	38
Figure 5.5	A screenshot of the Labview GUI interface. Source: Labview . . . . .	39
Figure 5.6	A screenshot of the Labview block diagram. Source: Labview . . . . .	40
Figure 5.7	Image of the GNU Radio Filter Design tool . . . . .	42
Figure 5.8	Image of the HackRF used to generate the offending signal . . . . .	43
Figure 6.1	A screenshot showing the iPython notebook code and related graphs generated for parsing GNURadio data . . . . .	45
Figure 6.2	Graph of the uncalibrated SDR total power values of Experiment I . .	46
Figure 6.3	Graph of the SDR calibrated noise temperature for Experiment I . .	47
Figure 6.4	Unfiltered data from the square-law detector collected in Experiment I	48
Figure 6.5	Filtered data from the square-law detector used in Experiment I . . .	49
Figure 6.6	Calibrated data from the square-law detector used in Experiment I . .	50
Figure 6.7	Figure showing both the SDR and square-law noise temperature data in Experiment I . . . . .	51
Figure 6.8	Graph of the calibrated total power from Experiment I while the matched load is submerged in LN2 between 350 and 450 seconds. . . . .	52
Figure 6.9	Graph of the calibrated total power with expected and actual sensitivity.	53
Figure 6.10	Graph of the calibrated total power over a period of fifteen minutes. .	54
Figure 6.11	Graph of the calibrated total power over a period of 15 minutes with a best fitted line. . . . .	55

Figure 6.12	Graph showing the unfiltered total power measurements of the software defined radio . . . . .	56
Figure 6.13	Graph showing the raw total power read from the square-law detector with an interfering signal. . . . .	57
Figure 6.14	Image showing the spectrum view of the SDR-based radiometer with no RFI mitigation. . . . .	58
Figure 6.15	Image showing the spectrum view from the SDR-based radiometer filtering the offending signal . . . . .	59
Figure 6.16	Graph showing the calibrated total power readings with the filter removing the offending signal . . . . .	60
Figure 6.17	Image of the offending signal being filtered out by the SDR. It can be seen that the signal is no longer visible. . . . .	61
Figure 6.18	Graph of the calculated $NE\Delta T$ , the proposed limit for the sensitivity of the radiometer, and the measured standard deviation with respect to filter bandwidth. . . . .	64
Figure 6.19	Graph of the total power measured and theoretical power versus the bandwidth of the measured signal. . . . .	65
Figure 6.20	Screenshot of the waterfall display showing the magnitude of the received power as a color, the frequency on the y-axis and time on the x-axis. . . . .	66
Figure 6.21	Side by side comparison of the waterfall display for when the matched load is submerged in LN2 and ice water. . . . .	67
Figure 6.22	Plot of the noise temperature of Experiment 1 with soil moisture percentage . . . . .	67
Figure 7.1	The key blocks used for creating a correlating radiometer in software. The key blocks is the USRP source, which allows us to address both daughter-boards and the ADD block which sums the signals. . . . .	72

Figure A.1 Blocks used for creating a total power radiometer in software. Source:  
GNURadio Companion . . . . . 75

## ACKNOWLEDGEMENTS

I would like to take this opportunity to express my thanks to those who helped me with various aspects of conducting research and the writing of this thesis. First and foremost, Dr. Phillip Jones for his guidance, patience and support throughout this research and the writing of this thesis. I would also like to thank Dr. John Basart who patiently spent many hours with me going over both the fundamentals and details with radiometers. I would like to thank Dr. Brian Hornbuckle for his continued support and for allowing me to utilize his radiometer, lab and students towards my research. Finally I would like to thank Dr. Mani Mina who not only was instrumental in my undergraduate career but continued his support into my graduate path as well. If it was not for Dr. Mina hiring me as the Chief Engineer of the Spacecraft Systems and Operations Lab, I would not be here today.

## CHAPTER 1. INTRODUCTION

This thesis explores using software defined radio (SDR) technology to develop a radiometer that has performance on par with that of traditional radiometer. In addition to demonstrating a SDR-based radiometer can achieve similar performance, in terms of sensitivity and stability, to a traditional radiometer, it is shown that the inherent flexibility of SDR technology allows implementing functionality beyond what a traditional radiometer typically provides. Furthermore, by reducing cost and increasing flexibility, SDR technology may become an attractive path for broadening the accessibility of radiometry to the general research community.

*Motivation.* Remote sensing refers to recording, observing and perceiving objects or events that are far away (i.e. remote)[Weng (2012)]. Since the object of interest is remote, we cannot physically interact with it using local measurement methods such as placing sensors or probes on the object. Remote sensing can be accomplished in a variety of ways and the following lists the basic approaches:

1. Visible light: Photography and Photogrammetry,
2. Thermal, Far infrared: Thermal Infrared Radiometry
3. Laser distance measurement: Lidar,
4. Radio Frequency (RF): Radiometry.

Each of these methods has an associated set of pros and cons, thus remote sensing often uses a combination of methods to paint a complete picture of an object. This thesis focuses on the apparatus used in radiometry to capture RF signals, called a radiometer.

Radiometry can be broken in to two methods; active or passive. An active system is one in which a radio frequency signal or pulse is generated and transmitted to the object of interest.

The reflection of this RF signal, or in some cases lack of reflection, gives us information about the object. A passive system is one in which no RF signal or pulse is generated. Instead, this type of radiometer simply listens to the RF energy that is naturally generated by the object or that may be reflected from another source, such as the Sun. Radiometers have been focused on Earth for such purposes as helping scientists better understand its water cycle by monitoring ocean salinity [Hardy et al. (1974)] and soil moisture [Liu et al. (2013)]. Radiometers such as these are already in service on satellites such as the Soil Moisture and Ocean Salinity (SMOS) satellite [McMullan et al. (2008)] launched by the European Space Agency (ESA). Additional applications of radiometry include: assessing vegetation health and observing celestial objects[Ulaby and Long (2014)].

*Problem Statement.* While radiometers have proved to be an excellent tool for remote sensing and have been used in research applications for over fifty years, they have not made it into wide spread use. This is due to the fact that many traditional radiometers have the following hurdles:

1. They are expensive,
2. They require advanced knowledge to implement and use,
3. They are typically built and designed for a custom application.

This thesis aims to help address each of these hurdles as follows. The use of commercial off the shelf (COTS) parts and solutions will help reduce cost and the need for a custom design. Software will be used to define key components of the radiometer that have traditionally been implemented in hardware and to ease adaptation to multiple applications. A user friendly graphical user interface (GUI) will help reduce the advanced knowledge required to implement and use the radiometer.

*Contributions.* The primary contributions of this thesis are:

1. Development of a software defined radio-based radiometer
2. Python based scripts for analyzing data generated by the radiometer

3. A Radio Frequency Interference (RFI) mitigation technique implemented using software defined radio technology

*Organization.* The remainder of this thesis is organized as follows. Chapter 2 gives a discussion of related works. Chapter 3 gives background on traditional radiometers and on software defined radios. Chapter 4 presents details on how software defined radio technology was used to implement a radiometer. Chapter 5 describes the experimentation setup used to verify and evaluate the operation of the implemented radiometer. Chapter 6 examines the results obtained from our performance evaluation experiments. Chapter 7 concludes this thesis and outlines avenues of future work.

## CHAPTER 2. RELATED WORKS

Three areas closely related to the work in this thesis are: digital radiometers, software defined radio based radiometers, and Radio frequency interference mitigation (RFI). This chapter first presents two classifications of digital radiometers (hybrid and direct sampling). Next, software defined radio based radiometers are discussed in their own section, as a third classification of digital radiometer. This chapter concludes with a brief overview of the topic of RFI, which is important to consider when deploying radiometers.

### 2.1 Digital Radiometers

A digital radiometer replaces portions of a traditional radiometer with digital components[Ruf and Gross (2010)]. Two types of digital radiometers include: hybrid and direct sampling.

*Hybrid.* A hybrid radiometer uses a mixture of analog and digital components[Skou and Vine (2006)]. Often the analog voltage output from the diode of a square law detector, which is used to indicate the total power observed, will be digitized.

*Direct Sampling.* A direct sampling radiometer can be considered a type of hybrid radiometer that directly samples the incoming RF signal and then uses digital signal processing techniques to extract total power information.

As an example, Iowa State University (ISU) owns a 1.4 GHz, dual polarization, correlating radiometer that uses direct sampling. It was built by the University of Michigan and put into service at ISU in 2006 [Erbas et al. (2006)]. This radiometer takes the RF signal and using analog components amplifies and filters the signal, and then sends it to an analog to digital converter. When the the ISU radiometer was built, an analog to digital converter (ADC)

that could sample accurately at 1.4 GHz were expensive and not easily obtainable. Since this radiometer was only interested in power information, it could under-sample at 1.4 GHz. The samples are sent to a Field Programmable Gate Array (FPGA) to extract power information. The correlation stage is another place where a radiometer could be digitized. [Fischman (2001)].

Both hybrid and direct sampling radiometers are designed to retain only the total power information contained in a RF signal. While measuring total RF power is the primary purpose of a radiometer, as it will be discussed later, retaining phase and frequency information can be useful as well.

## 2.2 Software Defined Radio Based Radiometers

Software defined radio based radiometers can be considered a relatively new subclass of digital radiometers. With the advent of software defined radios that are wildly available, their has been increasing interest in applying this technology to radiometers.

*Shirleys Bay Radio Astronomy Consortium.* The Shirleys Bay Radio Astronomy Consortium (SBRAC) made use of a software defined radio to restore a radio telescope used for radio astronomy. They attached a software defined radio to their eighteen meter radius dish to obtain astronomical information by observing the hydrogen line located at 1420.4058 MHz in the RF spectrum[Leech and Ocame (2007)]. Marcus Leech, who headed SBRAC, contributed software to GNURadio specifically to support radio astronomy applications. This branch of GNURadio was used as the software base used in this thesis [Leech (2006)].

While parts of the GNURadio software used in this thesis were derived from Marcus Leech's work, additional features were added such as offending signal mitigation, offending signal detection and a software implemented noise generator. Additionally, elements of the graphical user interface (GUI) were enhanced to aid in visualization and analysis data. For example, a waterfall display of a signal spectrum over time was implemented.

*Grand Valley State University.* In 2013 the University of Illinois and Grand Valley State University built a software defined radio based radiometer to listen to emissions from Jupiter[Behnke et al. (2013)]. They custom built the hardware portion of their software defined radio using an Analog Devices analog to digital converter (AD9460) and a Xilinx (Spartan-3E-500) FPGA.

They also implemented a RF front end to filter and amplify the incoming RF signal. The software side of their radiometer was composed of GNURadio and Python scripts for low-level communications with their software defined radio. The students reported on the project that their SDR based radiometer worked well to implement a higher level user interface. One aspect that differentiates the work in the thesis and Grand Valley State Universities work is that they build their own custom hardware for their software defined radio, while in this work, off the shelf components were used with an aim of making radiometers more widely accessible to the research community.

This section discussed two works that have explored using software defined radio technology in radiometry from the Shirley's Bay Radio Astronomy Consortium and from Grand Valley State University.

### 2.3 Radio Frequency Interference (RFI) Mitigation

When an RF signal generated from a source other than the object or phenomena of interest interferes (i.e. masks or contaminates) with the RF signal of interest to a radiometer this is referred to as radio frequency interference (RFI). Radio Frequency Interference (RFI) is a common problem with nearly all radiometers because they are highly sensitive receivers, thus even small unwanted signals can have a large negative impact on a radiometer based experiments. It is for this reason certain frequency bands have been designated protected frequencies for radiometer use by the international community. However, not all entities abide by these standards. For example, the satellite radiometer used by the Soil Moisture Ocean Salinity (SMOS) mission has had numerous issues with RFI [Kerr (2012)] skewing their data and in some cases making the data unusable for soil moisture measurements [Richaume (2012)].

The area of RFI detection and mitigation is still an active field of research [Forte et al. (2013)]. With respect to RFI detection, since radiometers typically do not retain spectral frequency information, statistical methods have been explored that look at variations in the received power to determine when RFI is occurring.

With respect to RFI mitigation, the use of the kurtosis statistic method[De Roo et al. (2007)] or polarization signature method. To mitigate the offending signal, mechanical filters

are used to selectively filter out the offending signals [Misra et al. (2012)].

While mechanical filters are an effective means for RFI mitigation, they add both weight and complexity to the radiometer. For example, multiple filters would be required to isolate and remove the bands that contain the offending signal(s). One idea this thesis explores is making use of frequency information and applying software-based digital filters for RFI detection and mitigation.

## CHAPTER 3. BACKGROUND

This chapter gives background information on the operation of traditional radiometers and on software defined radios. We begin by looking at the major components of a radiometer and how it measures power. Next the metrics used to measure the performance of a traditional radiometer are discussed. Then an overview of how software defined radios operate is given. Finally, we review the tools used to develop a software defined radio based radiometer.

### 3.1 Radiometer Basics

A radiometer is a device designed to measure thermal electromagnetic emission by a material media due to the electron agitation within the material.[Ulaby et al. (1981)]. This electromagnetic emission is the thermal noise of the object and can be correlated to the physical temperature of the object[Nyquist (1928)]. Because of this correlation, the amount of noise received is called the noise temperature and it is measured in Kelvin.

There are six stages common to all radiometers. They are:

1. Source (antenna or  $T_A$ )
2. Bandwidth ( $\beta$ ),
3. Amplification (Gain or  $G$ ),
4. Power detection ( $X^2$ ),
5. Integration ( $\tau$ ),
6. Output (Voltage, rQ or Kelvin).

Figure 3.1 illustrates how a signal propagates through a radiometer. First, the signal from the source enters the antenna,  $T_A$ . Next the signal is filtered to a set bandwidth,  $\beta$ . This filtered signal is then amplified by Low Noise Amplifiers (LNAs) by a gain of  $G$ . The power information is then extracted from the signal using a square-law detector,  $X^2$ . A square-law detector takes the input RF signal and produces a voltage that is proportional to the square of the voltage[Leinweber (2001)]. This voltage output from the square-law detector is then integrated to smooth the signal using an integration time of  $\tau$ . Finally the integrated voltage signal is then measured.

A non-physical object that is present in all radiometers is system noise, represented as  $T_N$ . System noise is noise that is generated from within the radiometer due to thermal agitation. A radiometer is designed to reduce the system noise as much as possible by using low-loss components and amplifiers that are low noise such as Low Noise Amplifiers (LNA).

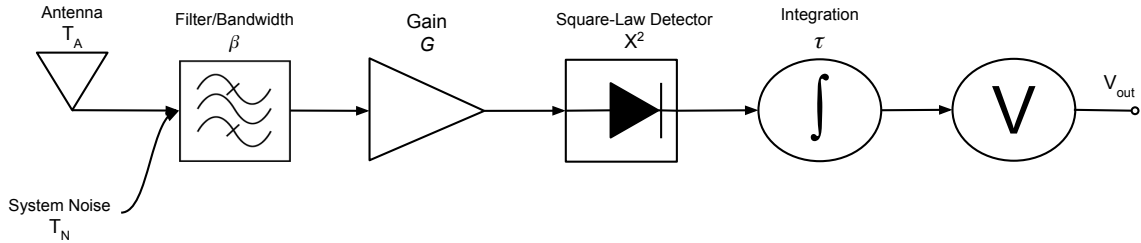


Figure 3.1 A total power radiometer block diagram

### 3.1.1 Power Measurement

As shown in Equation 3.1, the power measured by an ideal radiometer is equal to the product of the power received from the source ( $T_A$ ), the gain ( $G$ ) and the bandwidth ( $\beta$ ) of the radiometer, and the Boltzmann constant ( $k = 1.38 \times 10^{-23} J/K$ ).

$$P = k * \beta * G * (T_A) \text{ (watts)} \quad (3.1)$$

While the components of an ideal radiometer do not contribute noise power ( $T_N$ ) to the system, they do in a real radiometer. The impact of this internally generated and unwanted noise on the power measured by the radiometer is captured by Equation 3.2.

$$P = k * \beta * G * (T_A + T_N) \text{watts} \quad (3.2)$$

Gain ( $G$ ) and bandwidth ( $\beta$ ) are important design parameters of a radiometer. While a large gain is desired to amplify the source signal, the magnitude of the gain must be limited since it also amplifies the unwanted system noise ( $T_N$ ).

Since the bandwidth of the source signal is typically wide (ideally infinite), ideally one wants the radiometers bandwidth to be wide (large) as well. The two primary limiting factors are: 1) hardware limitations (e.g. LNA operating limits), and 2) unwanted signals located at a number of frequencies (e.g. radio communication signals).

*Low Noise Amplification.* The method used by most radiometer to mitigate the system noise contributed during the signal amplification is daisy chaining devices called Low Noise Amplifiers (LNAs). The total amount of amplification we can expect from  $N$  LNAs, is the sum of the gain values of each LNA shown in equation 3.3.

$$G_{total} = G_1 + G_2 + G_3 + \dots + G_{n-1} \quad (3.3)$$

A performance metric of a LNA is the noise figure ( $NF$ ). The noise figure gives us the difference between the actual noise output and an ideal amplifier with the same gain and bandwidth attached to a matched load at the standard noise temperature (290 K).

Another terminology used is the noise factor ( $F$ ). The noise factor shows how much the signal to noise ratio is degraded by the LNA. The noise factor is related to the noise figure shown in equation 3.4.

$$NF = 10 * \log_{10}(F) dB \quad (3.4)$$

For devices that are cascaded, the total noise factor is found by the Friis formula and results in equation 3.5. This equation allows us to examine how the noise figure, and also the noise

factor propagates through the cascaded LNAs.

$$F = F_1 + \frac{F_2 - 1}{G_1} + \frac{F_3 - 1}{G_1 G_2} + \frac{F_4 - 1}{G_1 G_2 G_3} + \cdots + \frac{F_n - 1}{G_1 G_2 G_3 \cdots G_{n-1}} \quad (3.5)$$

The key implication of this property is that the first LNA in the cascade contributes the most system noise. As a consequence, it is critical that the first LNA has the smallest noise factor , while the remaining LNAs provide a majority of the signal gain. While these LNAs provide higher gain they will have higher noise figures, but their contribution to the overall system noise is a fraction of the first LNA.

### 3.1.2 Radiometer Performance Metrics

Two criteria used to determine how well a radiometer performs are: 1) Sensitivity and 2) Stability. These criteria determine the smallest change in signal noise temperature (i.e. power) the radiometer can detect, and the amount drift power measurements have over an extended period of time.

*Sensitivity.* Sensitivity of a radiometer is the smallest change in power that can be detected. A radiometer must be able to differentiate between signal noise received by the antenna ( $T_A$ ) and the system generated noise ( $T_N$ ).

Two methods to quantify the sensitivity of a radiometer are: 1) experimentally, and 2) analytically. Experimentally, sensitivity can be computed as the standard deviation of the measured power (assuming a stable radiometer). Analytically, sensitivity can be computed as a function of radiometer properties. Equation 3.6 gives this relation. The term Noise Equivalent Delta ( $\Delta$ ) Temperature ( $NE\Delta T$ ) is often used interchangeably with sensitivity. As can be seen in Equation 3.6, sensitivity improves (i.e. becomes smaller) as the bandwidth ( $\beta$ ) and integration time ( $\tau$ ) of the radiometer increases[Ulaby et al. (1981)].

$$NE\Delta T = \frac{T_A + T_N}{\sqrt{\beta * \tau}} \quad (3.6)$$

The following example illustrates the impact system generated noise has on a radiometers ability to detect changes in signal noise. Lets assume we want a sensitivity of 1 K. If there is

no system generated noise (i.e.  $T_N = 0$ ) and the received signal at the antenna is 200 K (i.e.  $T_A = 200$ ), we can then calculate our receiver sensitivity by using equation 3.6. Lets assume a bandwidth of 10 MHz (i.e.  $\beta = 10 \times 10^6$ ) and that our integration time is 40 milliseconds (i.e.  $\tau = 0.04$ ). We can now take these values and put them in Equation 3.6 which results in Equation 3.7.

$$NE\Delta T = \frac{200 + 0}{\sqrt{10 \times 10^6 * 0.04}} = 1K \quad (3.7)$$

Equation 3.7 gives us a result of 1 K for our sensitivity which meets our goal. Because we do not have an ideal radiometer (i.e.  $T_N \neq 0$ ) lets assume our system noise added is 800 K (i.e.  $T_N = 800$ ). Assuming that our bandwidth ( $\beta$ ), our integration time ( $\tau$ ) and our antenna signal ( $T_A$ ) is the same, we can now apply Equation 3.6 which results in Equation 3.8. This results in a sensitivity of 5 K, which is five times higher than our ideal sensitivity of 1 K.

$$NE\Delta T = \frac{200 + 800}{\sqrt{10 \times 10^6 * 0.04}} = 5K \quad (3.8)$$

As can be clearly seen, system noise makes the job of detecting changes in signal noise more difficult[Skou and Vine (2006)].

Section 6.2.2 uses these two methods of finding sensitivity as a cross validation of the correctness of a SDR based radiometer.

*Stability.* Stability for a radiometer means that any fluctuations we see is a result of the source and not a change occurring within the radiometer. Lets examine Equation 3.2 which defines the total power the radiometer receives. If our bandwidth ( $\beta$ ), Gain ( $G$ ), system noise ( $T_N$ ), and Boltzmann constant ( $k$ ) are constant, then the system is stable. We can assume that our bandwidth is fixed and that our system noise is constant. This results in our Gain ( $G$ ) being the uncertain variable that may cause unwanted fluctuations[Evans and McLeish (1977)].

Radiometer instabilities are due to Low Noise Amplifier (LNAs) gain fluctuations. Two factors cause gain these gain fluctuations: 1) fluctuations in the LNA's voltage supply, and 2) fluctuation in the LNA's physical temperature.

The impact these gain fluctuations have on stability is given by equation 3.9. Where:

- $\Delta T_G$  is the noise temperature fluctuation,
- $\Delta G$  is the LNA gain fluctuation,
- $G$  is the gain of the LNA and,
- $T_{sys}$  is the combined antenna source ( $T_A$ ) and system noise ( $T_N$ ).

$$\Delta T_G = T_{sys} \left( \frac{\Delta G}{G} \right) \quad (3.9)$$

These gain fluctuations can be controlled by closely monitoring and controlling both the voltage and temperature of the LNAs. However, this adds levels of complexity to the radiometer, that may be impractical in some cases. As an alternative, modifications to the basic radiometer given in Figure 3.1 have been developed to compensate for these fluctuations. There are three common types of radiometers designed to account for gain fluctuations. They are: Dicke, Noise injection, and Polarimetric or Correlating radiometers.

*Dicke Radiometer.* Figure 3.2 shows the block diagram of a Dicke radiometer, which switches between the measurement of the source signal ( $T_A$ ) and a known reference signal ( $T_R$ )[Dicke (1946)]. By quickly switching between the source and reference signal at a frequency of  $F_S$ , a Dicke radiometer can reduce the impact of gain fluctuations on its stability.

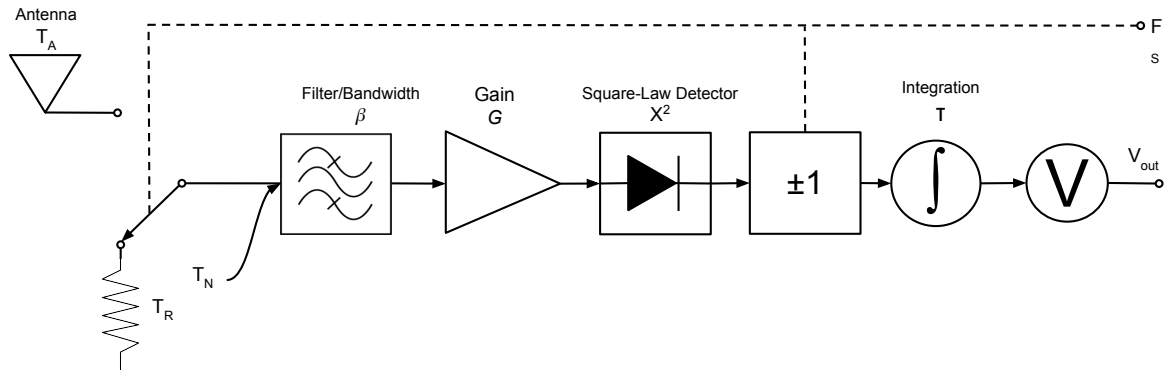


Figure 3.2 A block diagram of a Dicke radiometer

While a Dicke radiometer improves stability, it does so at the cost of not seeing the object of interest while it is measuring the reference signal. This reduces the sensitivity of the radiometer since the source signal is only observed for a fraction of the time.

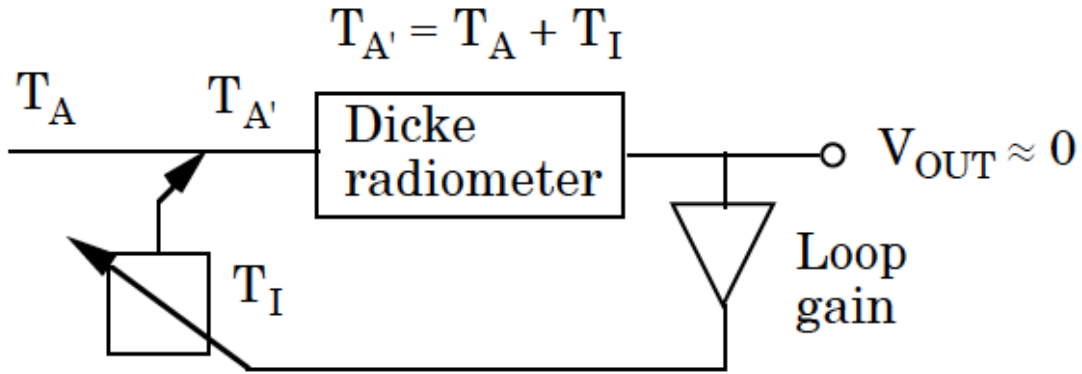


Figure 3.3 A block diagram of a Noise Injection radiometer

*Noise Injection Radiometer.* A noise injection radiometer is a variation of the Dicke radiometer, where a variable noise signal ( $T_I$ ) is injected into the RF chain as seen in Figure 3.3. The injected noise signal power is adjusted so when added to the source signal, their sum equals to the reference signal. This eliminates gain fluctuations, but increases system noise ( $T_N$ ) which reduces radiometer sensitivity.

*Polarimetric Radiometer* A polarimetric (or correlating) radiometer uses two polarized signals, referred to as vertically polarized (V-Pol) and horizontally polarized (H-Pol). In order to accomplish this, an antenna with dual polarization is used [Fujimoto (1964)]. Each polarized signal is fed into the radiometer and correlated. Because the source noise signal has polarization and the gain fluctuations does not, the gain fluctuations can be eliminated. This reduces gain fluctuations to increase stability, helping maintain sensitivity. However, this is at the cost of increasing radiometer complexity and price, since two identical receivers (one for each polarization) is required.

### 3.2 Software Defined Radios Basics

A Software Defined Radio (SDR) is a device that digitizes a received RF signal as soon as possible, and processes the digital representation of the signal using a computer, FPGA, or dedicated System on Chip (SoC). A canonical software defined radio architecture consists of a power supply, antenna, analog to digital converter, and a processing unit to carry out radio functions in software [Mitola (1995)]. An ideal software defined radio block diagram is shown in figure 3.4.

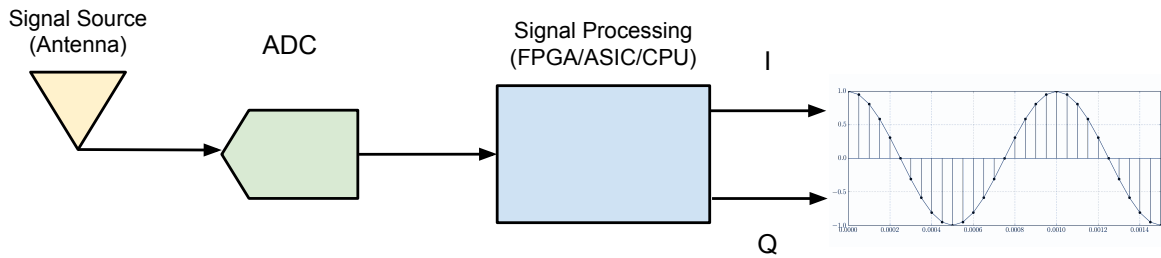


Figure 3.4 An ideal software defined radio

A SDR can perform certain hardware functions in software (e.g. filtering). This gives SDRs a high amount of flexibility because components that were normally performed in hardware can now be performed in software. Changes can be made by simply uploading new software or firmware to the system. This has a cost benefit as certain hardware components are no longer needed and changes made in software do not require additional hardware to be added, removed or modified.

A more realistic software defined radio is shown in figure 3.5, where two items have been added. First, an amplification of the signal (gain) is added to improve SDR sensitivity. Second, a mixer is often used to down-convert the high frequency RF source signal to a lower frequency so a less expensive analog to digital converter can be used. However, if the source signal frequency is already within the range of the analog to digital converter, then the mixer may be omitted.

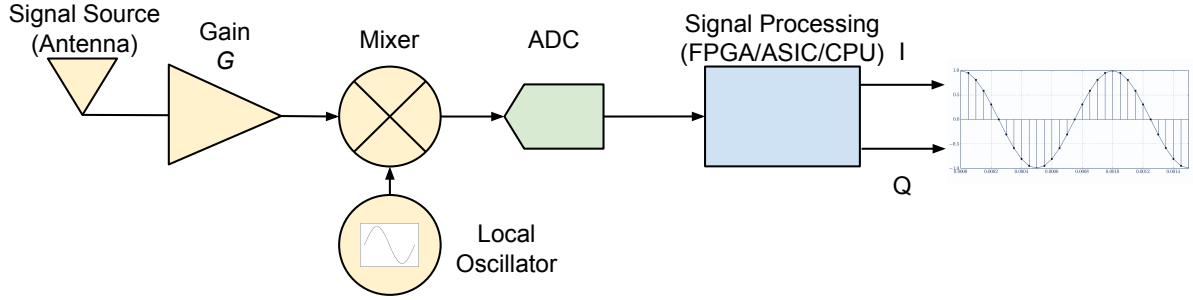


Figure 3.5 A typical software defined radio

*Software Defined Radio Applications.* Software Defined Radios (SDRs) can be for a variety of applications, but have been primarily used in the area of communications. Some examples of these applications include: mobile communications, wireless local area networks, personal area networks and digital broadcast. They appeal to applications where having the ability to change a modulation scheme or filter on the fly is desirable. In these respects, SDRs often outperform traditional hardware-only radios because of their ability to easily change their operations through software.

Early SDRs were expensive due to the cost of high speed analog to digital converters (ADCs) and high-end Field Programmable Gate Arrays (FPGA) that were required. In recent years, the cost of SDRs have decreased due to the cost of these key components decreasing. Also, while the cost of SDRs has gone down, their performance has increased. This has led to SDRs becoming feasible for use in many new ways [Jondral (2005)].

### 3.3 Software Defined Radio Development Platform

This section discusses the platform used to develop a software defined radio based radiometer. The hardware and software tools used are off the shelf. First, the hardware platform will be introduced, followed by the software platform.

### 3.3.1 Hardware Platform

The hardware platform selected for this work is the Ettus Research Group N200 SDR shown in figure 3.6. The N200 has the following features that made it desirable for our specific application:

- Dual 14-bit ADC,
- 25 MHz bandwidth per channel,
- Modular daughter-board system for RF front end.

Its flexible architecture and ability to support a large bandwidth made the N200 an ideal hardware platform for the software defined radio based radiometer development.



Figure 3.6 The USRP N200 from Ettus Research (Image from Ettus Research Website - [www.ettus.com](http://www.ettus.com))

When selecting the hardware for this thesis, the requirements defined section 4.1 were examined. The bandwidth requirement was a deciding factor for hardware selection. It was decided that a minimum bandwidth of 20 MHz was desired. The 14-bit ADC was not a defined requirement, but was deemed to provide an adequate level of resolution. The N200 has a flexible architecture through the use of daughter-boards.

Figure 3.7 shows the overall architecture of the N200 SDR. A daughter board directly receives the RF signal and then outputs analog I (in-phase) and Q (quadrature phase) signals that are then sampled by the N200 14-bit A/D converter.

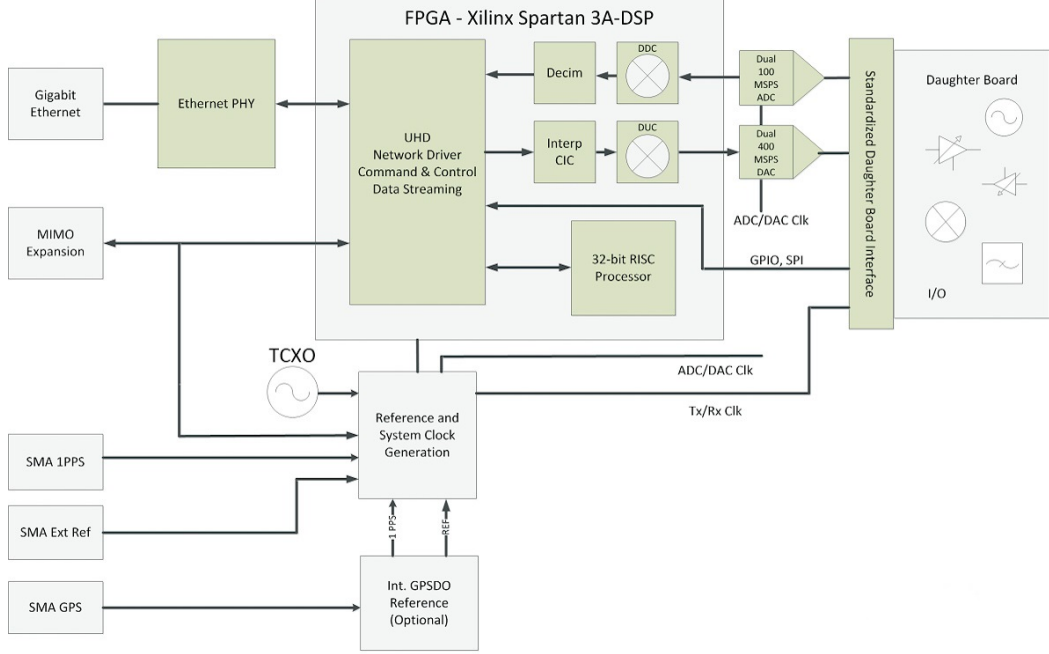


Figure 3.7 A block diagram of the Ettus N200 SDR. (Image from Ettus Research Website - [www.ettus.com](http://www.ettus.com))

*The DBSRX2 Receiver.* The daughter board selected for this work was the DBSRX2 shown in figure 3.8. This daughter board is receive only, and operates between 800 MHz and 2400 MHz, which includes the frequency band required for this work (1400 MHz - 1425 MHz).

The DBSRX2 has the RF hardware needed to transform the received RF signal into phase and quadrature phase outputs. This includes a programmable gain amplifier, a direct-conversion converter, a mixer, and finally a band-pass filter. Figure 3.9 provides a block diagram of the DBSRX2. First, the signal received is amplified by the Programmable Gain Amplifier (PGA). The PGA is can be configured by the software. Next, the signal goes into a direct-conversion integrated circuit (a Maxim 2112). This integrated circuit directly converts the RF signal into analog I (in-phase) and Q (quadrature phase) values and is composed of an integrated mixer and band-pass filter.

These analog I and Q values are then sent to the analog to digital converter to be digitized. The IQ values are transmitted as differential signals to minimize noise. Once digitized, the digital I Q values are sent to a FPGA to be processed, and then sent to the PC for soft-ware based signal processing.



Figure 3.8 The DBSRX2 daughter board from Ettus Research (Image from Ettus Research Website - [www.ettus.com](http://www.ettus.com))

### 3.3.2 Software Platform

There are two pieces of software that are used with the software defined radio: 1) the firmware that is used in the FPGA of the N200, and 2) the software running on the host PC.

The firmware provides low level processing of the signal before being sent to the software located on the PC. It also provides a link for controlling key aspects of the software defined radio, such as gain, bandwidth and the center frequency. This firmware comes pre-loaded into the FPGA by Ettus Research, and can be upgraded using tools provided by Ettus Research.

The software on the host PC performs signal processing on the I/Q data. GNURadio was selected to be this software. GNURadio is an open source software package designed for software defined radio application development. It provides a GUI framework to create an interactive environment for the user, and is well supported by the N200 hardware.

GNURadio uses a combination of Python and C++, where Python handles the high level interface and C++ is used to implement drivers and low level interfaces to the hardware. This combination allows for a system that is easy to use, but still meets the demanding performance required for handling large amounts of data.

GNURadio also has a rapid development tool called GNURadio companion (GRC). GRC is a simple to use graphical system for designing and building radio components in software.

An example of GRC is shown in figure 3.10.

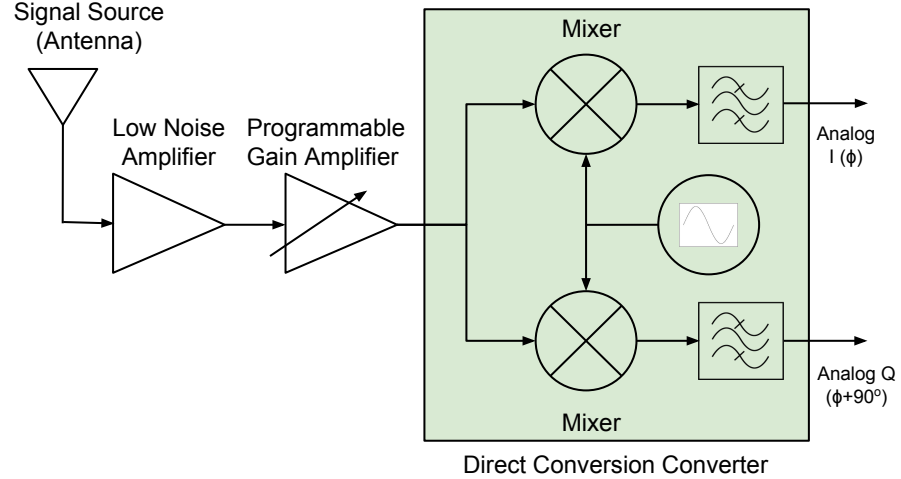


Figure 3.9 Block diagram of the DBSRX2 daughter board.

GNURadio Companion provides common functions, such as signal sources, signal processing and signal sinks, as blocks that can be picked and placed on the screen. Once placed, the blocks can be wired up, much like LabView, and the flow of data can be controlled in this fashion. GNURadio Companion also includes blocks that allow for building a GUI interface, which can be used to display data and control the software defined radio.

If a block does not exist, it can be created. Because GNURadio uses Python, users can use this powerful and flexible language to build new blocks that can be imported into GRC.

Using GNURadio and GNURadio Companion, a software defined radio can be rapidly built with little programming experience. The excellent support of the hardware selected, and the ease of use made it an ideal development tool for building the necessary software for our software defined radiometer.

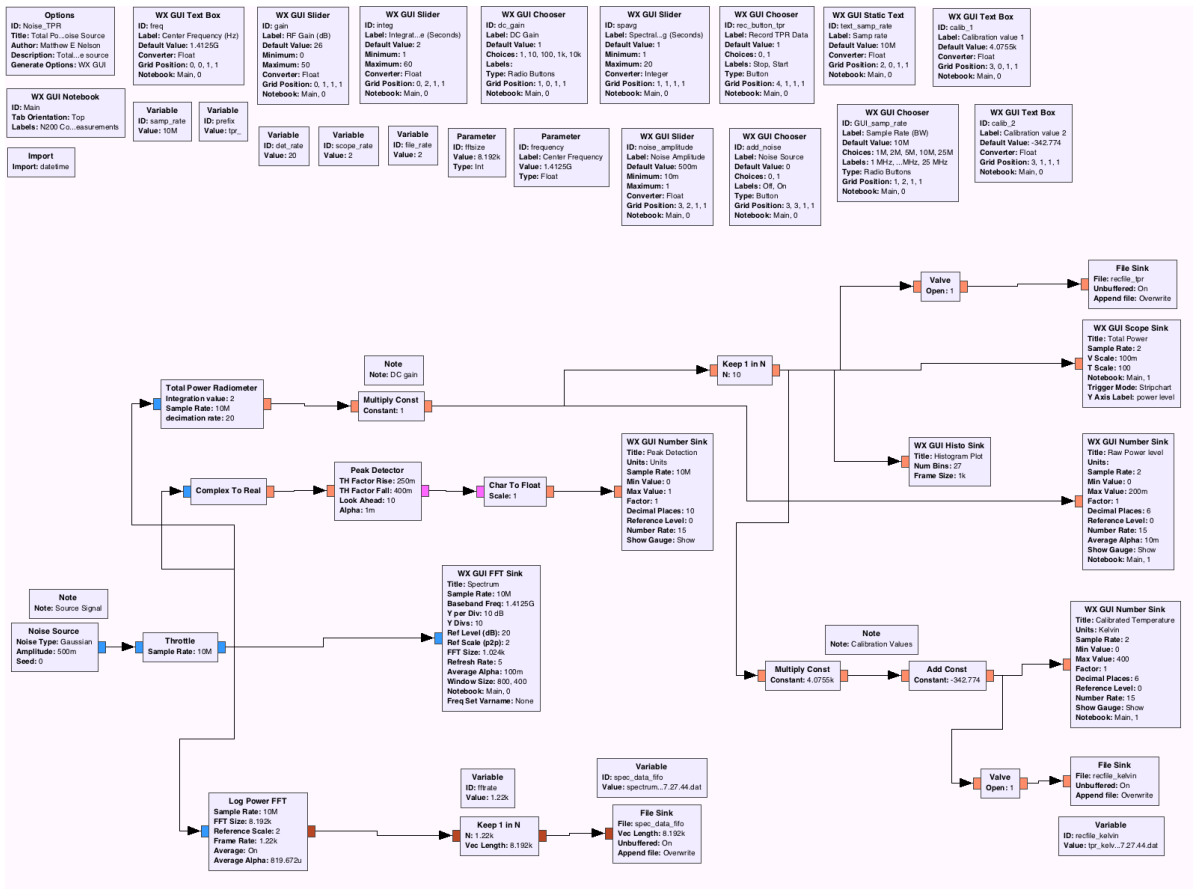


Figure 3.10 A screenshot of the GNURadio Companion editor program. Source: GNURadio

## CHAPTER 4. SOFTWARE DEFINED RADIOMETER IMPLEMENTATION

This chapter examines the implementation of a software defined radio based radiometer. First we will examine requirements of both a traditional radiometer and a digital radiometer. Next we will map the traditional radiometer components discussed in chapter 3 to their digital counterparts. Finally a high level overview of a software defined radio based radiometer will be given.

### 4.1 Requirements

This section discusses the hardware and software requirements used to drive the selection of the hardware and software platforms use to implement our software defined radio based radiometer.

*Hardware Requirements.* The capabilities of existing traditional radiometers were the primary driving force in setting the requirements of our hardware development platform. Dr. Brian Hornbuckle from the Electrical and Computer Engineering and Agronomy department at Iowa State University was consulted with respect to key specifications of his radiometer. Additionally, the specifications of other radiometers were examined.

Table 4.1 summarizes the specification of three parameters that were decided upon for selecting our hardware development platform, based on our investigation. This lead to the selection of the N200 software defined radio platform with a DBSRX2 daughter board from Ettus Research as our platform. Section 3.3 provides more in depth information on the hardware used and why it was selected.

*Software Requirements.* Since an objective of this work was to help make radiometers more

Table 4.1 Required Radiometer performance

Parameter	Value	Units
Minimum bandwidth	20	MHz
Operational frequency	1400 - 1420	MHz
$NE\Delta T$ (sensitivity)	1	Kelvin

wildly accessible to the general research and education communities, a requirement of the development software was ease of use. Additionally, the user interfaces developed with these software tools needed to be easy to use, while providing sufficient computing efficiency for the signal processing required for radiometry.

GNURadio met the stated requirements. It includes a supplemental software package called GNURadio Companion (GRC), which uses a graphical interface for creating a radio environment. GNURadio and GRC are discussed in greater detail in Section 3.3.2.

## 4.2 Mapping Traditional Radiometer Functions to a Software Defined Radio Based Radiometer

The use of a software defined radio (SDR) to implement a radiometer requires mapping components of a traditional radiometer to SDR-based technology. This section presents the mapping of three such components for implementing our SDR-based radiometer. These components are: 1) power measurement, 2) integration, and 3) filtering.

### 4.2.1 Power measurement

A traditional radiometer uses a device called a square law detector to measure power. It transforms an input signal into an output voltage whose square is proportional to the input signal power. Figure 4.1 shows a simple circuit diagram. Mathematically it takes an input signal ( $x$ ) and gives an output ( $y$ ) as the square of the input as shown in equation 4.1.

$$y = x^2 \quad (4.1)$$

The software defined radio based radiometer operates in the same manor as a traditional radiometer. The input signal, represented as I (in-phase) and Q (quadrature-phase), is squared

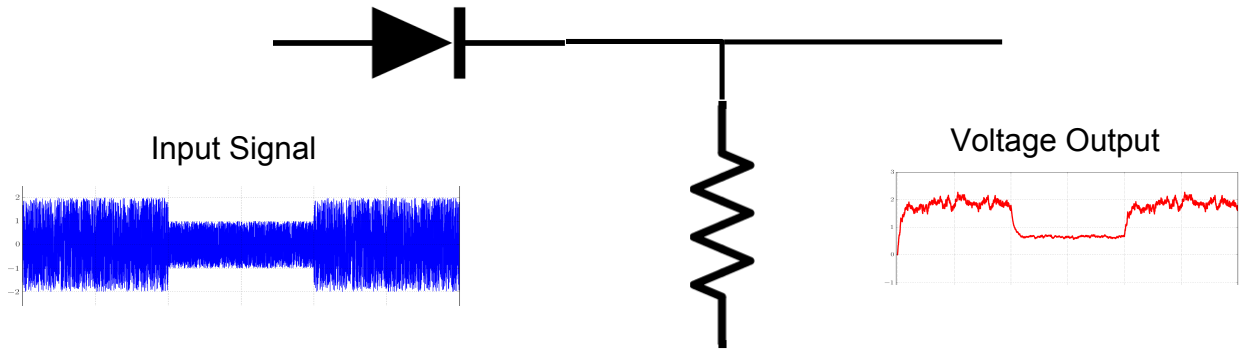


Figure 4.1 A simple diagram of a square-law detector.

and summed to produce an output ( $P_{out}$ ). Equation 4.2 gives the mathematical representation of a software defined radio based radiometer implementation of a square law detector[Rashid et al. (2011)].

$$I^2 + Q^2 = P_{out} \quad (4.2)$$

Figure 4.2 shows the block within GNURadio Companion that performs the function of total power measurement. In Figure 4.2, the block labeled as A performs mathematically the power detection as shown in Equation 4.2. Block C decimates the data to reduce the sample size and thus reduce the file size of the data.

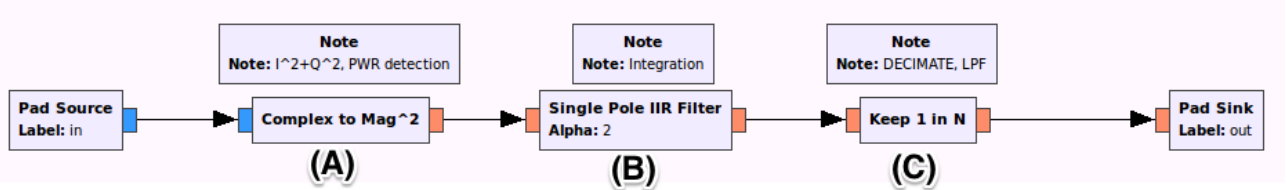


Figure 4.2 A block diagram of the power detection, low pass filter and decimation block used for total power measurements.

For both a traditional radiometer and a SDR based radiometer the output of this total power information will fluctuate rapidly. To smooth this signal we will pass this signal through a low pass filter which is shown in Figure 4.2 as block B. Filtering will be discussed in the next

section.

#### 4.2.2 Data filtering

Output from the square-law detector is noisy due to the rapid fluctuations in the signal. Figure 4.3 shows an example of this raw output. This makes detecting small changes in power difficult (i.e. hinders sensitivity).

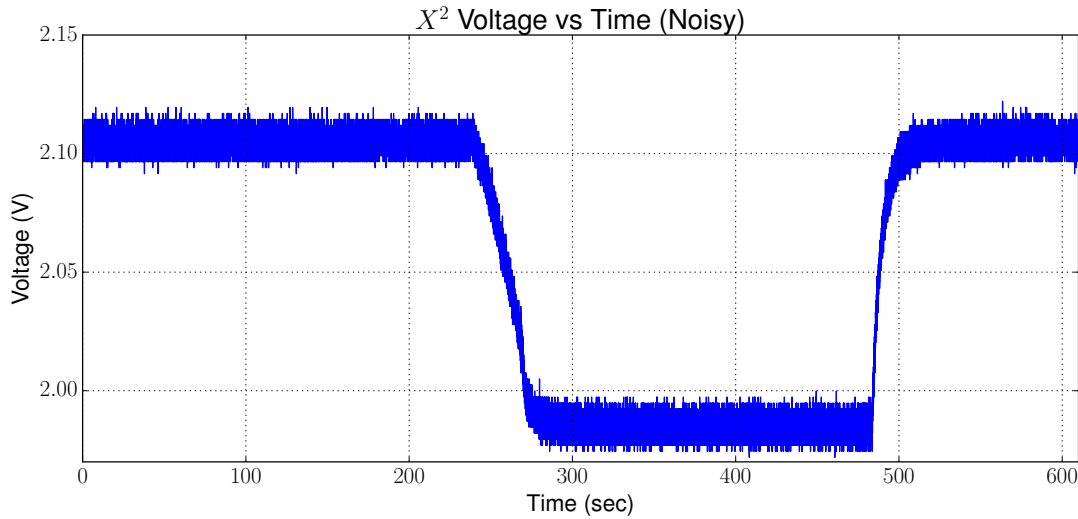


Figure 4.3 Power measurements from a square law detector before filtering

A traditional radiometer will use an integrator, which is equivalent to a low pass filter, to smooth the output from the square-law detector. This low pass filter is implemented as a simple RC circuit as shown in Figure 4.4.

This low pass filter allows us to reduce the noise and this results in Figure 4.5.

This RC filter is described by the Laplace transform of its impulse response. This RC filter is shown in Equation ??here  $K$  is the gain of the filter,  $\tau$  is the time constant of the filter and  $s$  is the Laplace transform variable.

$$\frac{\text{Output}}{\text{Input}} = K \frac{1}{\tau s + 1} \quad (4.3)$$

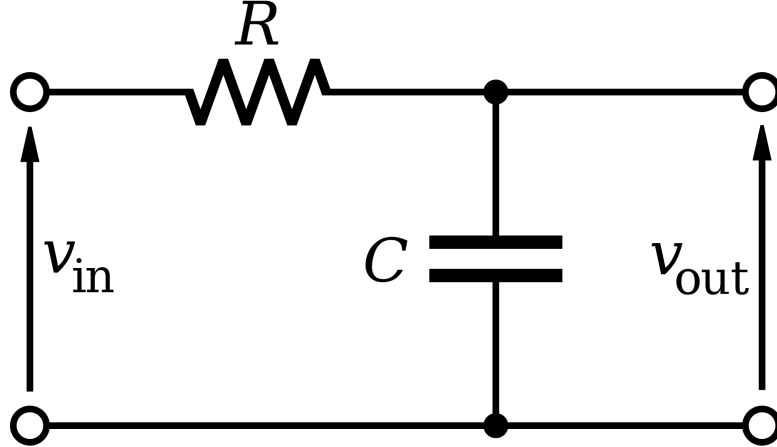


Figure 4.4 A simple RC circuit.

We can now look at the impulse response of this filter as shown in Figure 4.6. Figure 4.6 shows an impulse function used as the input to a RC filter.

To implement this low pass filter as a digital filter, a single pole Infinite Impulse Response (IIR) filter is used. We can examine how a IIR filter is identical to a RC filter by looking at the impulse response of this filter as we did with the RC filter impulse response.

A single pole IIR filter is also known as a recursive filter as the mathematical expression used to describe this filter is a recursive function shown in Equation 4.4.

$$y[n] = a_0 * x[n] + b_1 * y[n - 1] \quad (4.4)$$

In Equation 4.4, our discrete output ( $y[n]$ ) is defined as the input signal ( $x[n]$ ) and is added to the previous sample calculated. The coefficients,  $a_0$  and  $b_1$  then define the impulse response of the filter.

Figure 4.7 shows the discrete impulse input given to the system and the output response. This response is calculated using Equation 4.4.

It can be seen that Figure 4.7 is identical to Figure 4.6 except that it is using discrete values. Therefore are single pole IIR filter functions identically to a RC low pass filter.

GNURadio includes a program that allows us to define our filter and it will generate the coefficients and taps needed for our filters. Chapter 6 goes into more depth on this program.

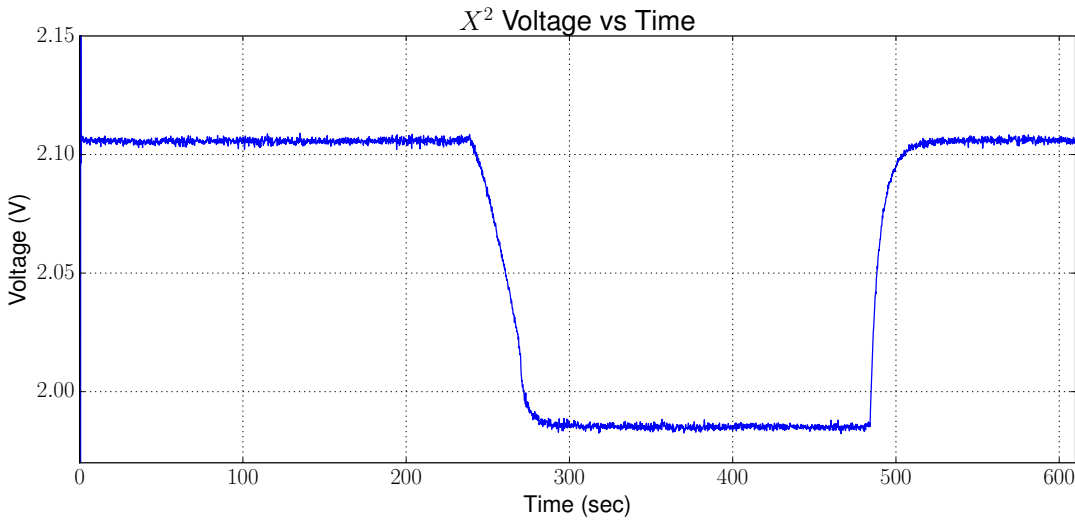


Figure 4.5 Power measurements from a square law detector after filtering

#### 4.2.3 Bandwidth limitation

A traditional radiometer will use filters to define the bandwidth of the radiometer. A software defined radio based radiometer however uses the sampling rate to define the bandwidth. This sample rate may be adjusted but will be limited by the computational power available. The higher the sample rate, and therefore the more bandwidth observed, the more computational power needed.

Additional filtering can be created and used in a software defined radiometer. These filters are often created using either IIR or FIR filters. The most efficient method is to restrict bandwidth by setting the sampling rate. However, these filters can be used to filter out either a narrow band of frequencies or to temporarily reduce the overall bandwidth. A common application of these additional filters is to remove an offending signal detected by the software defined radio based radiometer. This method of mitigating signal interference will be discussed in chapter 6.

### 4.3 Software Defined Radio Based Radiometer Control System

Like a traditional radiometer, the SDR uses an antenna to look at the target of interest. SDRs still use an amplification to improve the sensitivity of the SDR. After that stage though, a software defined radiometer is different. A SDR will sample and generate I and Q values that represents the signal. From there, this data is sent to a computer to be processed. We can then use this information to calculate the total power of the signal. In addition, we can manipulate the signal in other ways such as applying a filter to filter out an unwanted source.

A traditional radiometer will be designed with bandwidth and integration time fixed. While changes can be made, it requires changes to the radiometers physical hardware. A Software Defined Radio (SDR) based radiometer however can have both the bandwidth and the integration time changed. These changes can even be made while the radiometer is operating since both operations happen in the digital domain.

Because these values have an impact on the performance of a SDR based radiometer, it is important to have access

Next we will now look at how we control the software defined radiometer using the software detailed in chapter 3, section 3.3.2 in defining the radiometer. We will also look at how the data is displayed and stored in the software defined radiometer.

#### 4.3.1 Control of the SDR based radiometer through GNURadio

A GUI is designed to allow control of several key functions of the SDR based radiometer. This GUI is shown in Figure 4.8.

This interface is able to control several key aspects of the radio hardware within the SDR. This has the impact of affecting the behavior of this software defined radiometer as well. Through this we can control: frequency, sample rate (Bandwidth), integration time, and the gain on the DBSRX2 daughter board. We will no look at how these controls impact the performance of the radiometer.

### 4.3.2 Impact of the Controls Related to Radiometry

Having the ability to control these key aspects of the software defined radiometer allows us to affect the performance of the radiometer. The  $NE\Delta T$ , equation 3.6, discussed in chapter 3 outlines what some of these changes affect in a radiometer.

$\beta$  can be changed by changing the sample rate of the SDR. The sample rate effectively controls the bandwidth in which the SDR is operating at. This also gives us a band-pass filter as well, since the SDR will not respond to frequencies outside of this bandwidth.

$\tau$  is the integration time for the radiometer. This parameter is set by the user through the GUI and allows us to change the integration time in seconds.

We will now look at how this data is displayed by the SDR based radiometer.

### 4.3.3 GNURadio Data Display

The information from the software defined radio can be displayed through GNURadio to show a number of things. Since we have both frequency and magnitude information we can display this information. We are able to also display the information that shows the total power that is being seen by the radiometer as well.

We are not limited to just total power from the radiometer. If the radiometer has been calibrated, those calibration points can be entered and GNURadio can calculate the calibrated noise temperature.

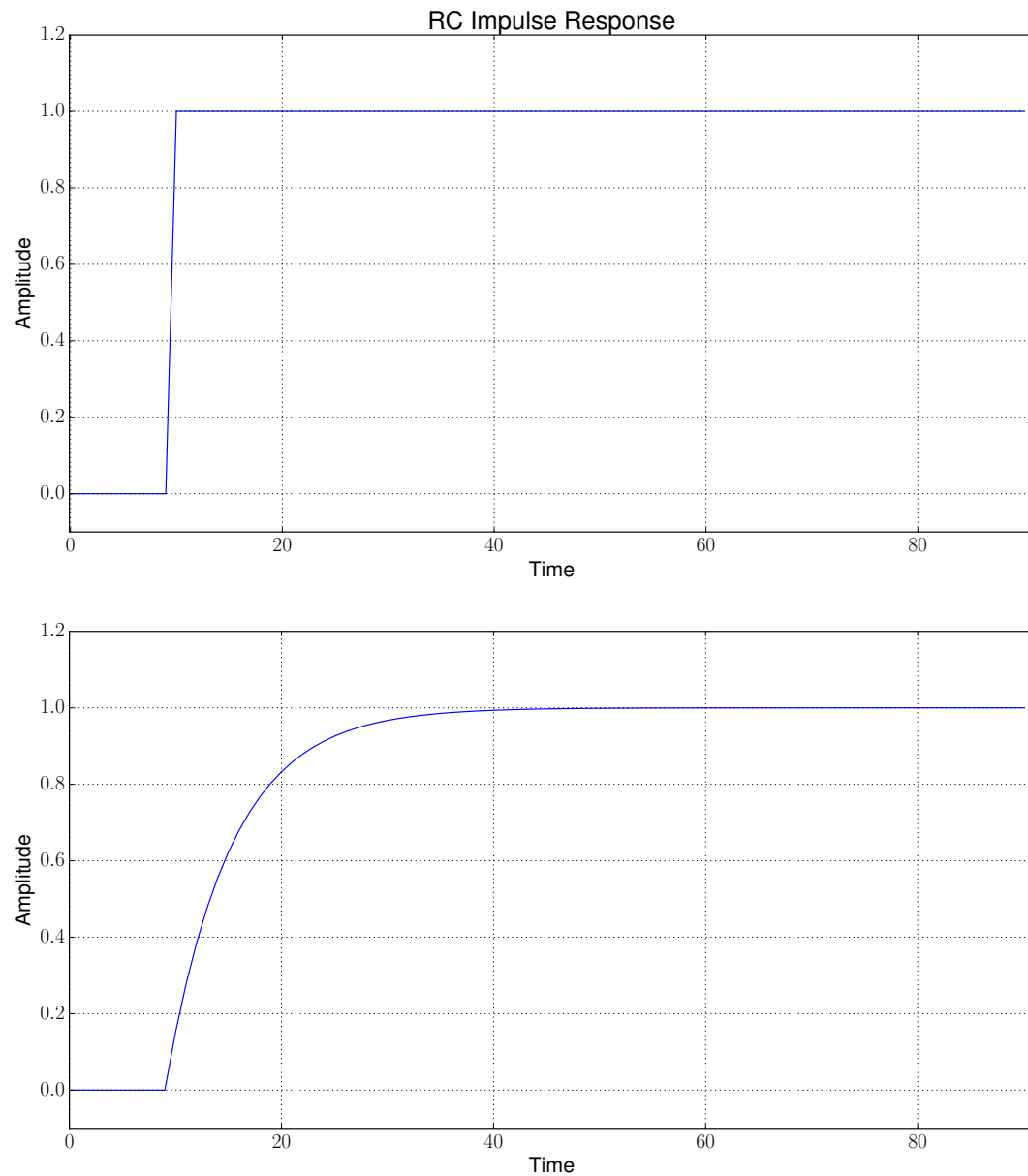


Figure 4.6 Impulse input and the response of a RC low pass filter

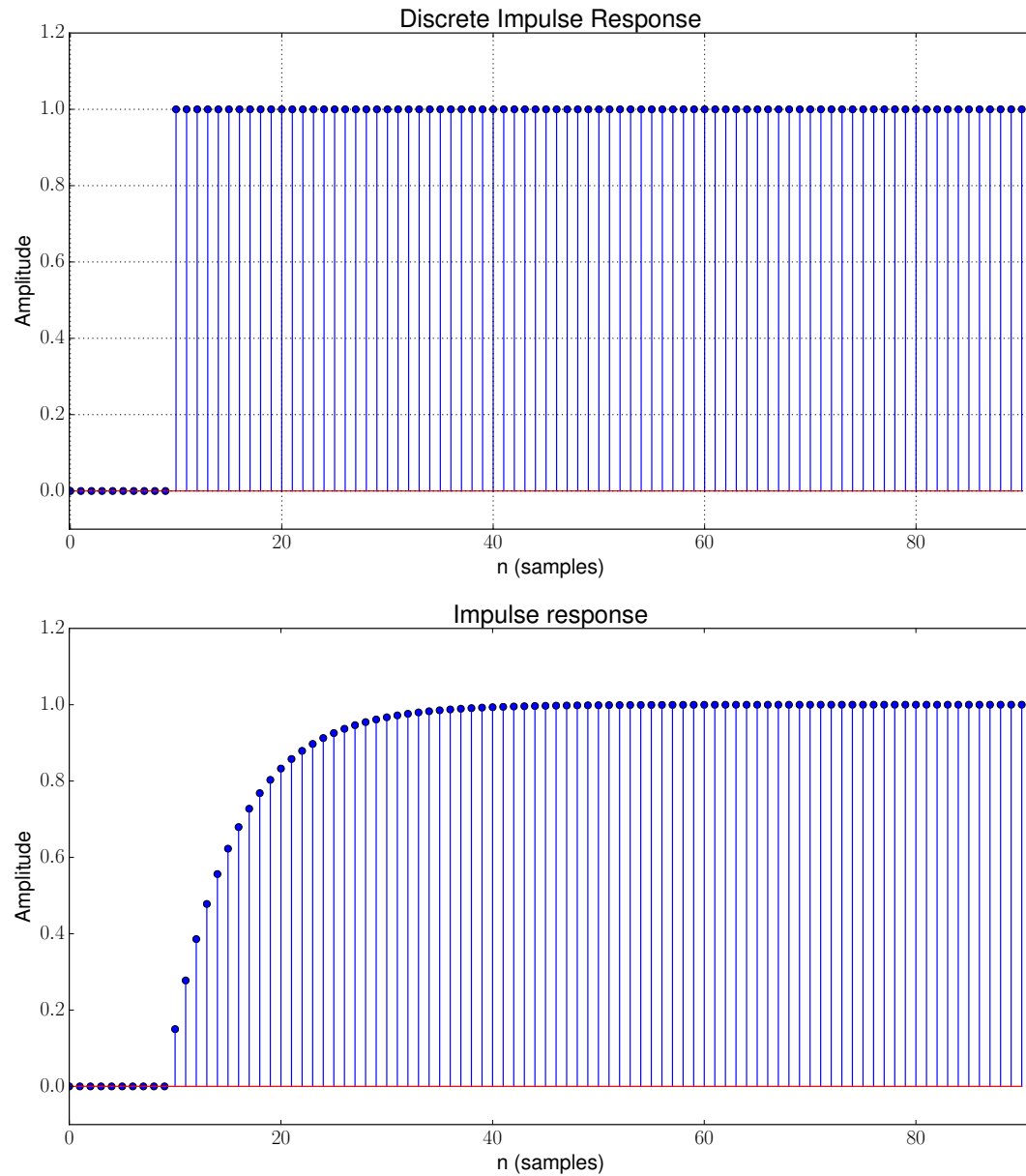


Figure 4.7 Impulse input and the response of a RC low pass filter

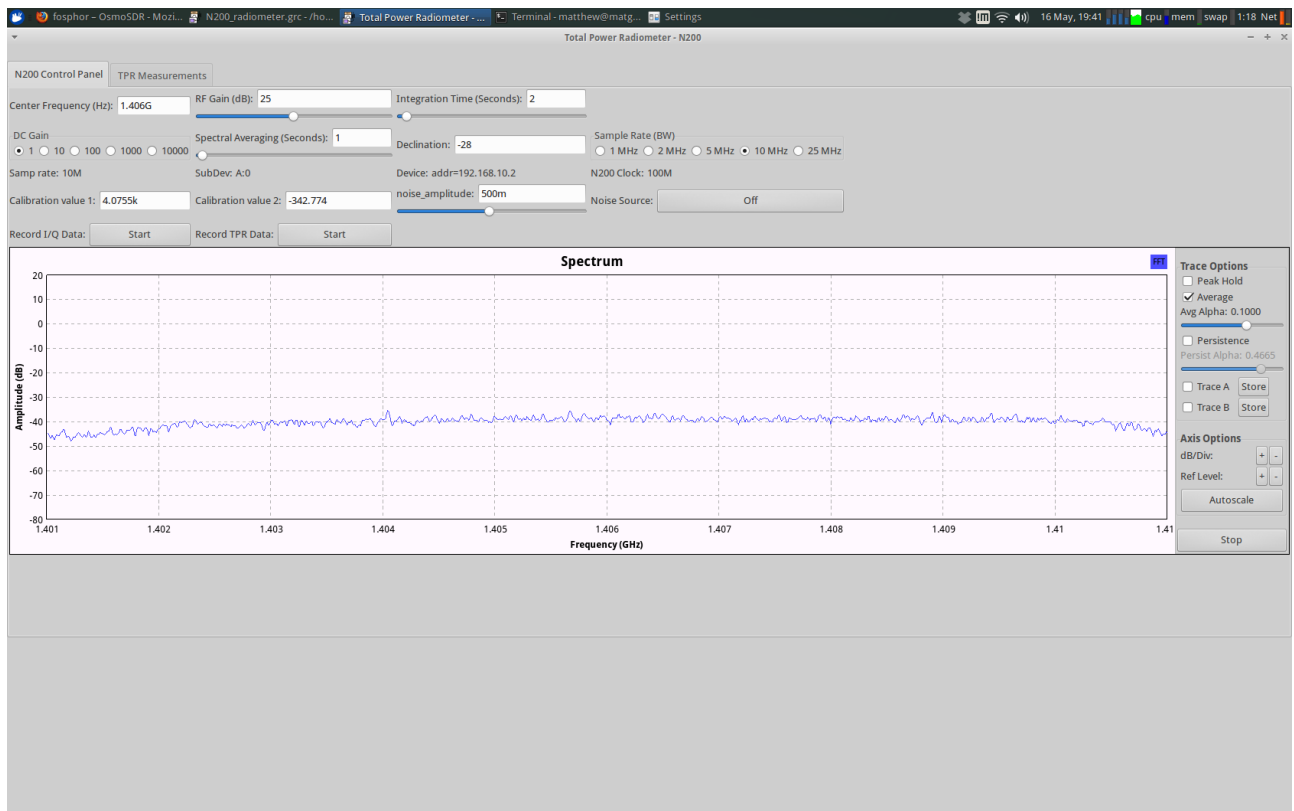


Figure 4.8 A screenshot of the interface made for communication with and controlling the software defined radio

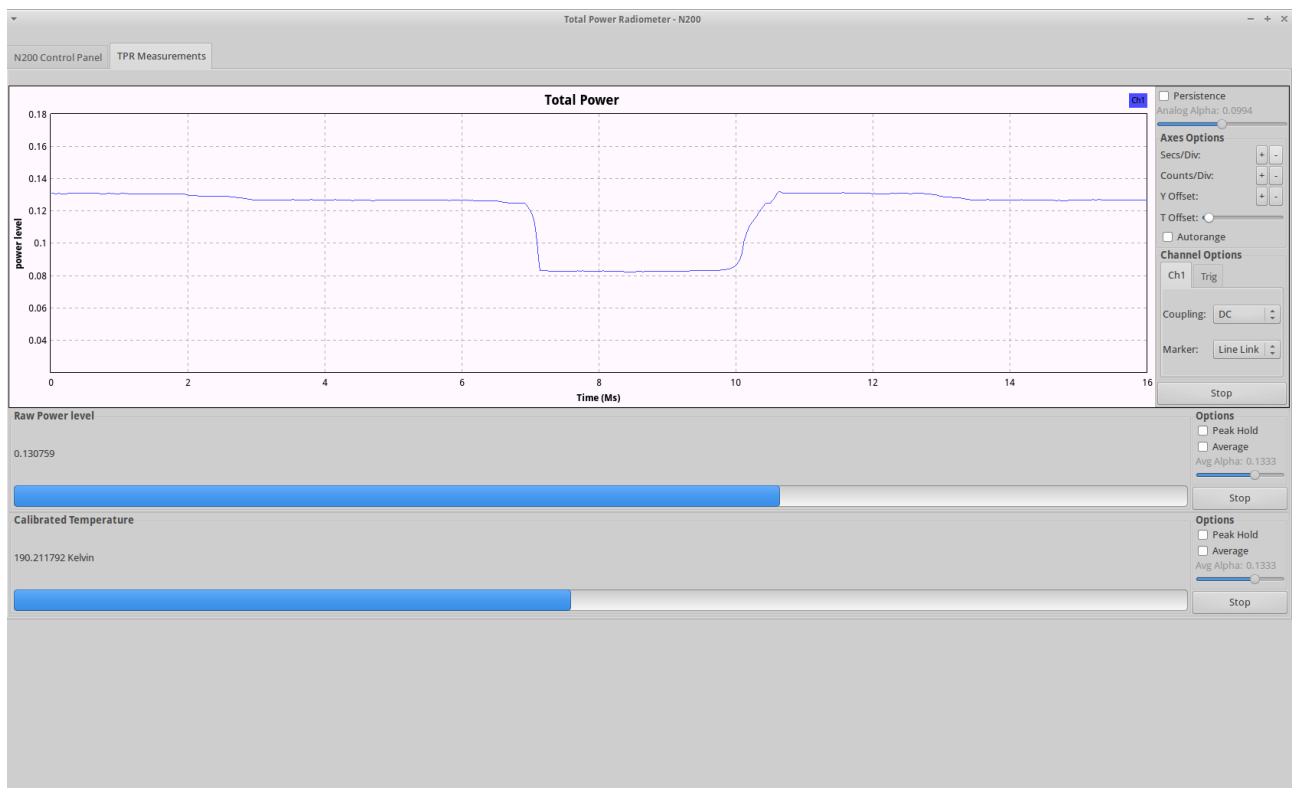


Figure 4.9 A screenshot showing the ticker tape display for the total power readings. In addition, raw and calibrated noise temperature is shown below.

## CHAPTER 5. EVALUATION SETUP AND EXPERIMENTAL DESIGN

The experiments outlined in this chapter are used to demonstrate and verify that a software defined radio (SDR) base radiometer can perform on par with a traditional radiometer. In addition, these experiments are designed to demonstrate that a SDR based radiometer can provide additional functionality not typically found in traditional radiometers.

Four experiments are described. Experiment one verifies our SDR-based radiometer by comparing its operation to a square-law detector, a device typically used within a traditional radiometer. Experiment two evaluates the sensitivity and stability of our SDR-based radiometer. Experiment three will evaluate our SDR-based radiometer's ability to mitigate an interfering signal in comparison to the behavior of a traditional radiometer in the presence of an interfering signal. Experiment four's purpose is to further examine the impact of our frequency based notching approach for RFI mitigation on radiometer sensitivity.

### 5.1 Experiment I - Software Defined Radiometer Verification and Calibration

This experiment is designed to verify our SDR-based radiometer functions as expected. Its behavior is compared against a square-law detector, which is commonly used in traditional radiometers. To verify the results of the information that the software defined radio is obtaining a square-law detector is used to measure the power of the incoming signal in parallel to the SDR-based radiometer. This signal is split using a power divider so that the information will be the same to both devices. This allows us to verify the software defined radio with a proven system.

### 5.1.1 Experimental setup

Figure 5.1 shows a block diagram of the experimental setup. A matched load is used to simulate our source signal. This matched load is then submerged in temperature baths. These baths use Liquid Nitrogen (LN2) which is known to boil at 77 Kelvin and an ice water bath which is known to be at 273.15 Kelvin. The temperature of these could easily be monitored and maintained. The load was submersed in each bath for a minimum of 2 minutes to allow for it to reach the same temperature as the bath. The physical temperature of this matched load is then the noise temperature the radiometer sees and can be used to calibrate the radiometer.

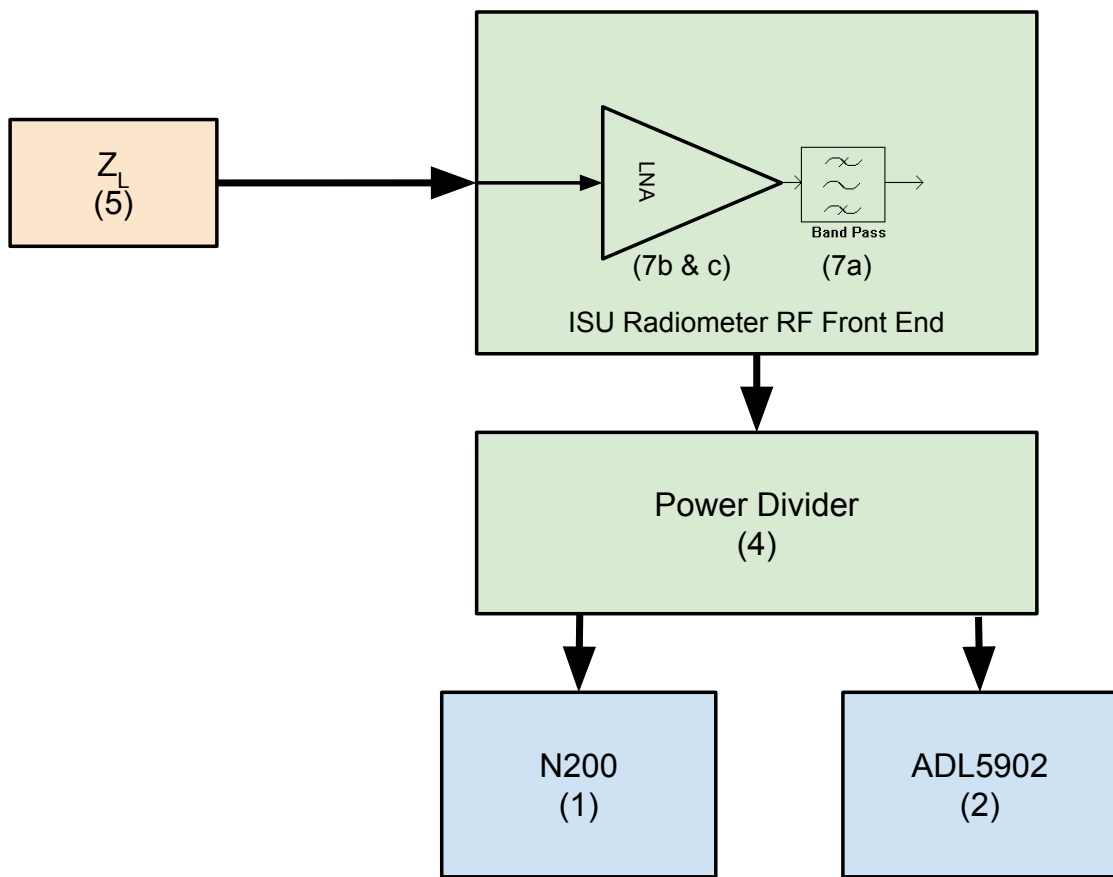


Figure 5.1 Block diagram of Experiment 1 setup. Source: Matthew E. Nelson

The radiometer RF front end provides the amplification needed for our experiments. Figure 5.2 shows an image of the RF front end used with the LNAs and band-pass filters marked. After

the signal has been amplified we divide that signal between the ADL5902 square-law detector and the N200 Software defined radio. The N200 is then connected to a personal computer running XUbuntu Linux and GNURadio.

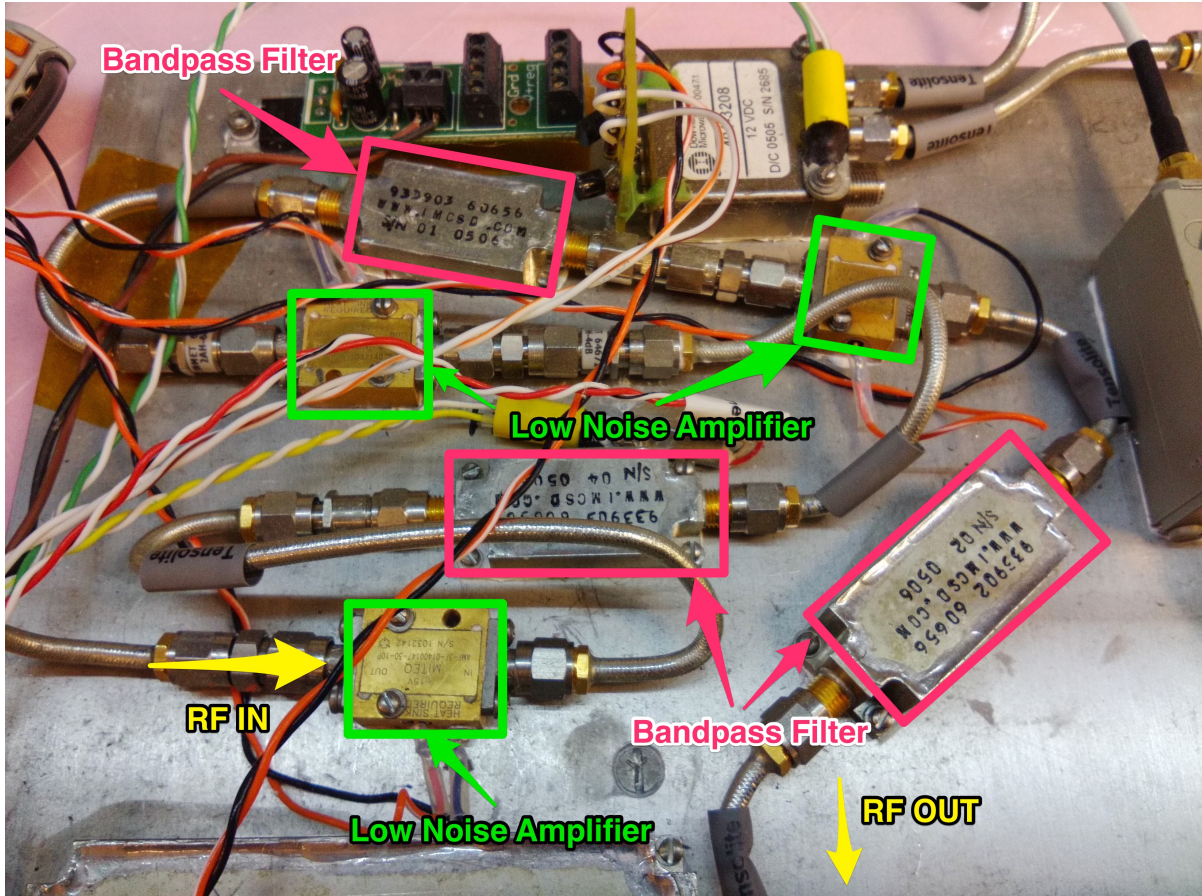


Figure 5.2 The radiometer RF front end with LNAs and band-pass filters used in the experiments. Source: Matthew E. Nelson

The following hardware was used and has also been marked on Figure 5.1:

1. N200 Software Defined Radio with DBSRX2 Daughter-board
2. ADL5902 Square-law detector
3. National Instruments USB-6009 Data Acquisition Unit
4. ZN2PD-20-S+ Power Divider

5. 50-ohm matched load
6. Rigol DP832 Power Supply
7. Radiometer RF Front End
  - (a) 4 x Integrated Microwave Bandpass filters (1400 - 1425 MHz)
  - (b) 2 x Miteq AMF-3F-01400147-30-10P LNA
  - (c) 1 x Miteq AMF-2F-01400147-04-10P LNA

### 5.1.2 Data Collection

Two sets of data are produced with this experiment. First, data is generated from the software defined radio using GNURadio. Second, data is generated from a data acquisitions device that is attached to the square-law detector. Data from each is stored to a local computer running the appropriate software.

*Software Defined Radio Data.* The data from the software defined radio is stored in files generated from GNURadio. GNURadio uses a sink block to output the data to either a screen, socket connection such as TCP/IP or a file. As shown in Figure 5.3, a file sink block is used to output the data to a file. The flow of data to this sink is controlled by a valve block. This allows for the user to turn on and off recording of the data.

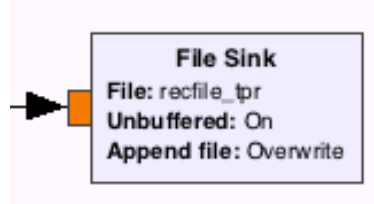


Figure 5.3 The File Sink block used in GNURadio. Source: GNURadio

There are two types of files that the SDR generates. The first type of file is the I (in-phase) and Q (quadrature phase) data points. This file is stored in little-indian format as complex values. Due to the sampling rate, it is not uncommon for this file to grow quite large, usually several gigabytes of data for a 10-15 minute run. However, this file can then be feed back

through GNURadio later to be played back if needed, and it contains the information needed to completely recreate the signal.

The second file type is the total power values generated from the total power block in GNURadio. A diagram of this block can be found in Appendix A (Figure A.1), and its source code can be found in Appendix A. This file also uses a little-endian format, however this file only has real values. This file is also much smaller than the file that contains the I and Q data points. A typical file size is 50 - 100 kB for a 10 to 15 minute run.

*Square-law detector data.* A square-law detector outputs information as an analog voltage that is linearly proportional to the RF power measured. The Analog Devices ADL5902 is a single Integrated Circuit (IC) that contains a square-law detector and necessary amplification for the output signal and is shown in Figure 5.4 . This device operates from 50 MHz to 9 GHz and can detect power as low as -60 dBm. The output voltage from the square-law is amplified to a range from zero to five volts with a calibrated output of 53 mV/dB.

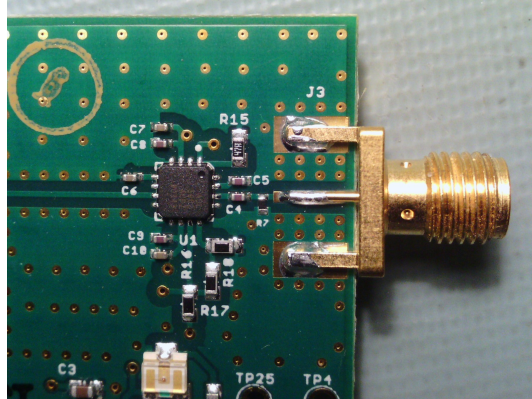


Figure 5.4 The ADL5902 IC on a demonstration board.

To capture the voltage output from the ADL5902, a data acquisition unit (DAQ) is used. The National Instruments USB-6009 DAQ unit was selected as it met the requirements for an easy to use yet high enough resolution to obtain accurate information. The USB-6009 unit has 8 analog inputs that can sample at 48 KSPS with a resolution of 14-bits.

To use the USB-6009 a fairly simple Lab View program was created to obtain, display and store the data from the ADL5902. This program retrieved the information from the USB-6009 and stored the data in both Labview's binary format and in a more human friendly ASCII

format. The USB-6009 then connects to a host computer through the USB interface. A GUI program, shown in Figure 5.5, is then used to control and display the data. This made obtaining the data and using the device straightforward.

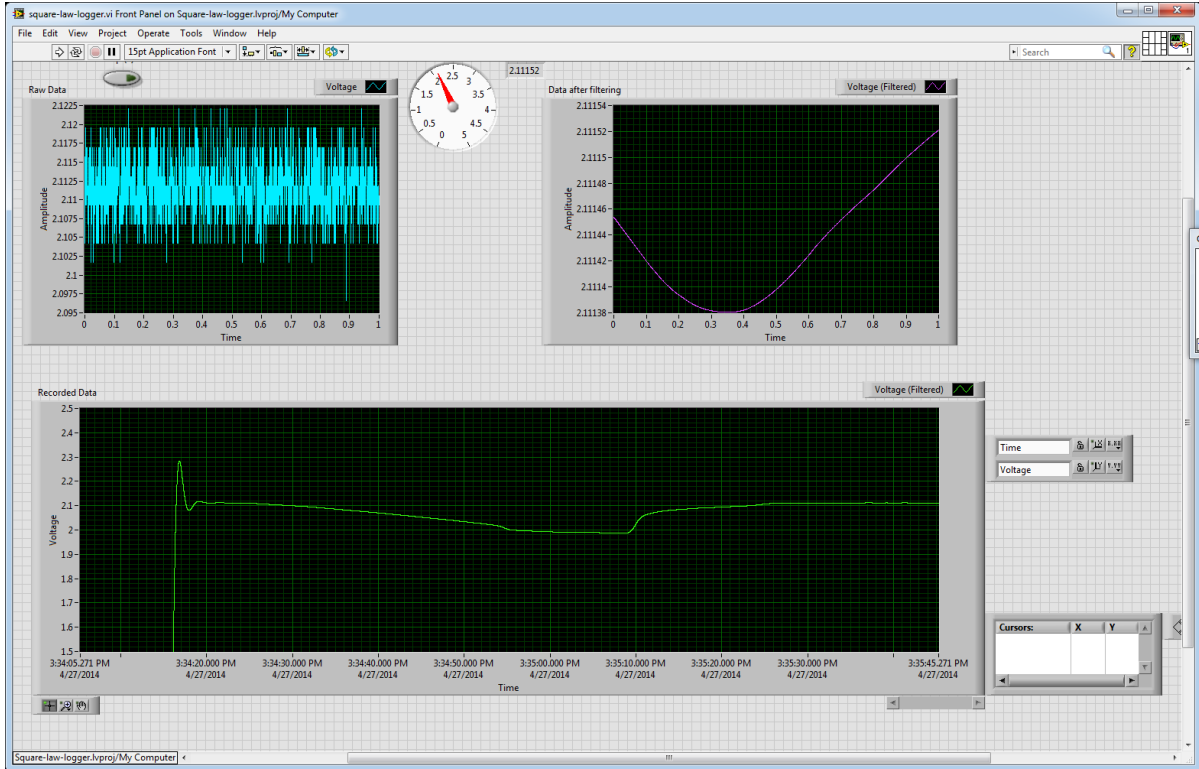


Figure 5.5 A screenshot of the Labview GUI interface. Source: Labview

For rapid development, the National Instruments DAQ assistant was used to quickly configure and setup the USB-6009. Labview also includes blocks that allows us to easily record the data to a file and to use a low pass filter. These blocks made up most of the program and resulted in a program that was quickly made. Figure 5.6 shows the blocks used and the wiring of the blocks.

## 5.2 Experiment II - Verification of sensitivity and stability

In this experiment we will verify the sensitivity and stability of a software defined radiometer. This experiment will verify that a software defined radiometer is able to meet the expected sensitivity and stability within an acceptable range.

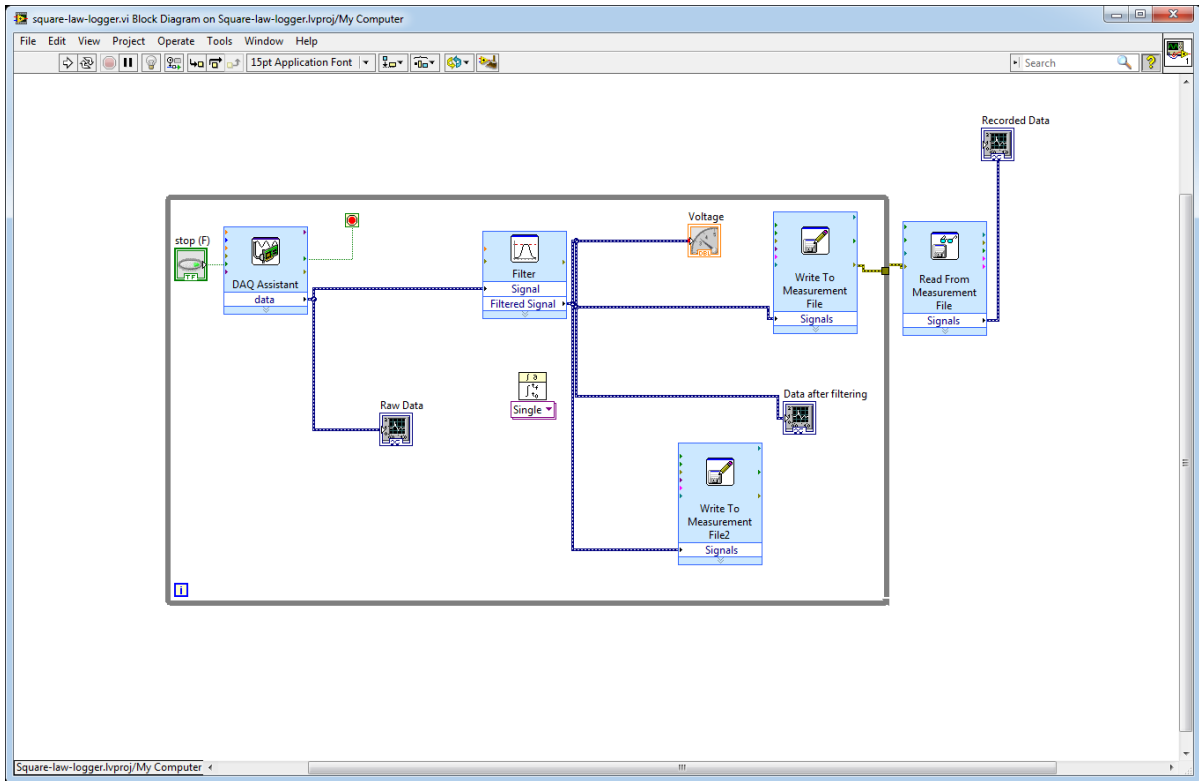


Figure 5.6 A screenshot of the Labview block diagram. Source: Labview

### 5.2.1 Experimental setup

The experimental setup used for experiment two is the same experiment as outlined in section 5.1.1.

### 5.2.2 Data Collection

The data collected for this experiment was the total power measurements made from the software defined radiometer. These measurements uses the same method as outlined in section 5.1.2.

## 5.3 Experiment III - Interfering Signal Mitigation

In this experiment we generate an interfering signal and then mitigate the signal using a software defined filter. A square-law detector is hooked up in parallel to measure the same

signal but is not provided with a mitigation mechanism. We then compare the two signals to verify that the SDR-based radiometer can mitigate the interfering signal, while continuing to still make useful total power measurements.

This experiment was designed to determine whether or not a SDR-based radiometer can cope with an interfering signal. This test injects a known signal at 1.406 GHz to interfere with the normal operation of the radiometer. The amplitude of this signal is then incremented and decremented at various times in the test. This was done to reflect a possible real world scenario and to make it easy to identify the interfering signal with the square-law detector which only measures power.

In order to mitigate the offending signal, a filter is designed to remove the offending signal. The design of the filter used a program that is part of the GNURadio software package, called the GNU Radio Filter Design tool. Figure 5.7 shows a screen shot of this tool when designing the band-reject filter for this application. This tool generates filter values (also called taps) that GNURadio will use for defining the filter. The GUI program shown in figure 5.7 allows us to interactively create a filter. Because this tool is part of the GNURadio package, it also includes a command line interface to the program. This allows us to call the program from within GNURadio to integrate this functionality into our SDR-based radiometer.

### 5.3.1 Experimental setup

The setup for this experiment is similar to the setup outline in section 5.1. In addition a second software defined radio was added to inject an offending signal into the RF signal chain. This software defined radio was configured to operate as a signal generator to create the offending signal.

Our signal generator is the HackRF One (or just HackRF), shown in figure 5.8. This SDR is cheaper, and has lower specifications than the Ettus Research N200 used as the SDR-based radiometer. However, it suits our needs for the purpose of a signal generator.

The HackRF generates a sinusoidal wave at a fixed frequency, and the signal amplitude changed at different times during the experiment. This is controlled from a program called *osmocom\_siggen*. Osmocom was originally developed to communicate with OsmocomSDR hard-

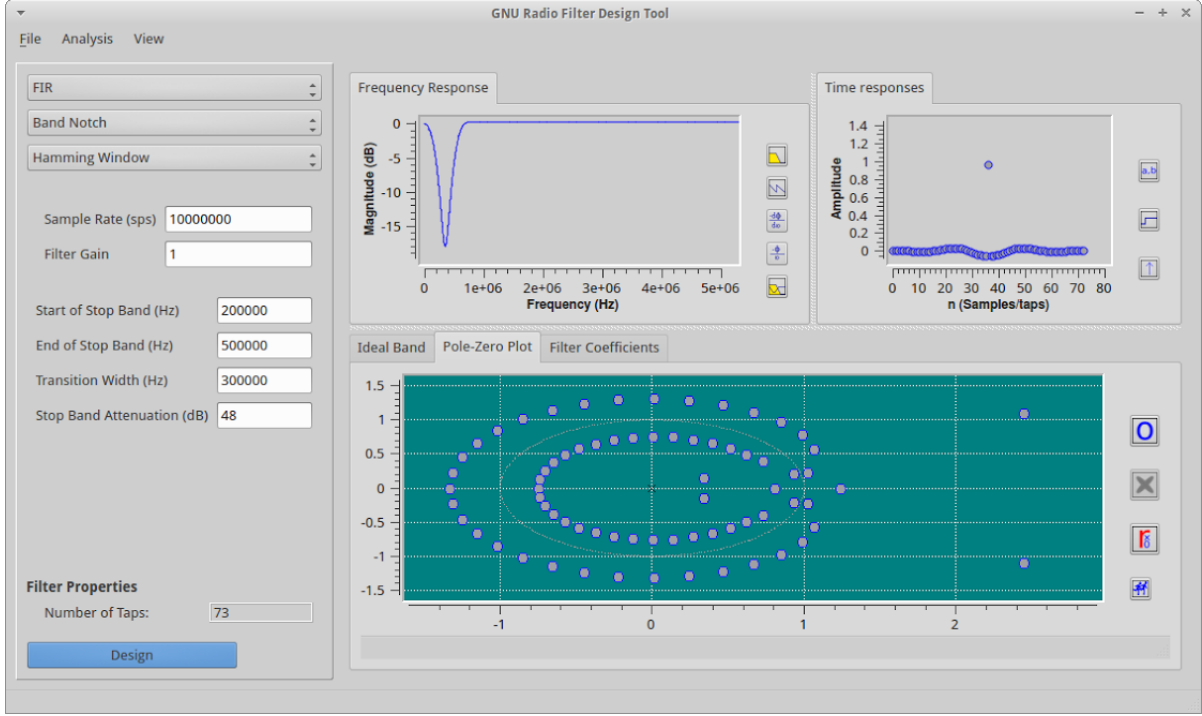


Figure 5.7 Image of the GNU Radio Filter Design tool

ware. However, it has been expanded to include the HackRF and Ettus Research hardware. The *osmocom\_siggen* program provides a GUI to set the frequency, amplitude, type of the signal generated.

### 5.3.2 Data Collection

The data collected for this experiment includes both the total power measurements from the software defined radiometer and the square-law data. Section 5.1.2 explains in detail the setup and configuration of the equipment used to collect this data.

## 5.4 Experiment IV - Performance impact of interfering signal mitigation

In this experiment we examine the impact of filtering an interfering signal on the sensitivity of the SDR-based radiometer and how reducing our overall bandwidth affects our total power received to the radiometer.

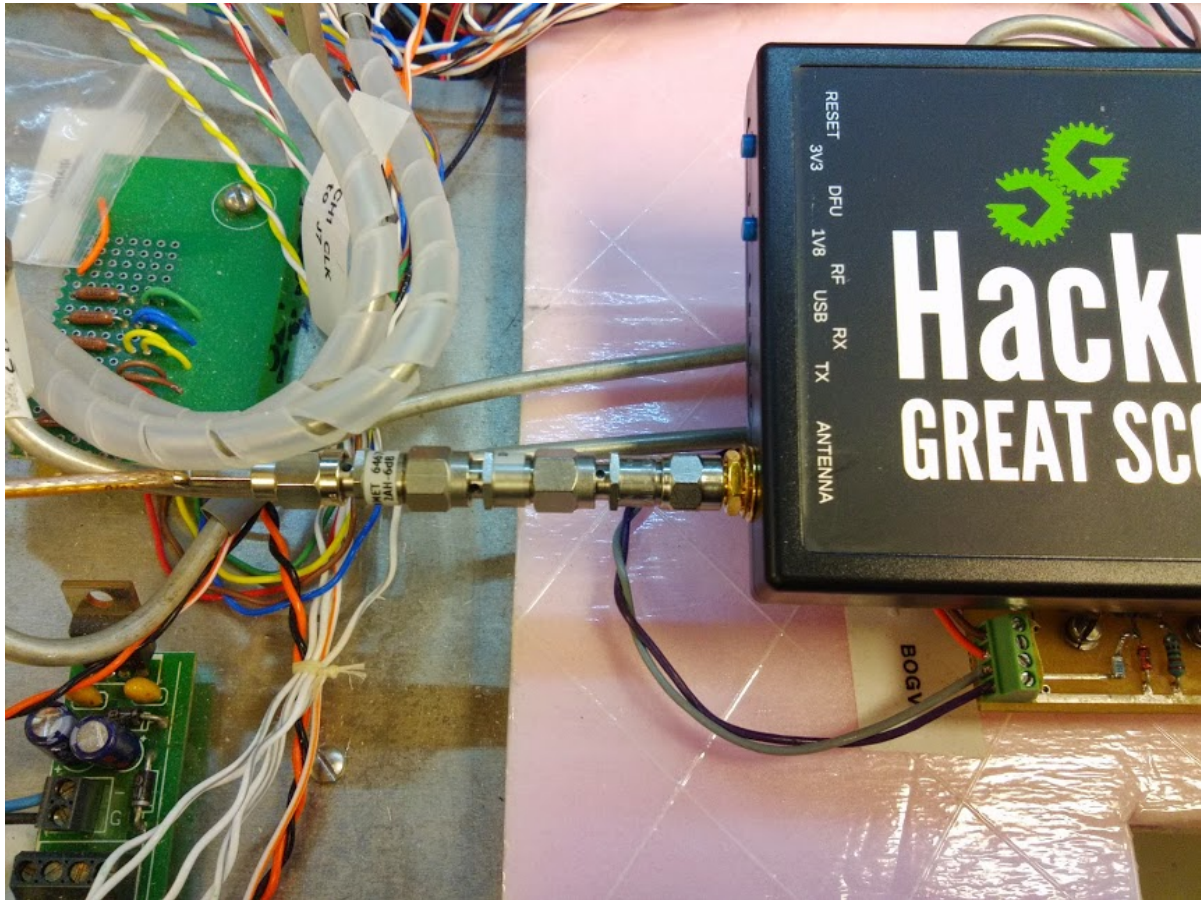


Figure 5.8 Image of the HackRF used to generate the offending signal

#### 5.4.1 Experimental setup

In this experiment we setup our experiment as outlined in section 5.3.1. The rest of the data collected is done by the analysis of the data collected.

#### 5.4.2 Data Collection

The data collected for this experiment is the total power reading measurements obtained from the software defined radio. This data is identical to the method used in section 5.1.2.

## CHAPTER 6. RESULTS AND ANALYSIS

This chapter presents the results obtained from the experiments outlined in Chapter 5. We discuss the analysis of the results and what was learned from each experiment. This chapter concludes with a trade off analysis between SDR-based radiometer and a traditional radiometer in terms of cost and weight.

### 6.1 Experiment I - Software Defined Radio Based Radiometer Verification and Calibration

As outlined in Chapter 5, Section 5.1, this experiment verifies the operation of a software defined radio based radiometer. This is done by performing experiments that are similar to the verification and calibration methods used for a traditional radiometer. We compare our results to those of a square-law detector receiving the same signal.

#### 6.1.1 Data Collected

For this experiment, total power measurements were collected from the software defined radio based radiometer and the square-law detector. This data is then calibrated using the known physical temperature of the matched load. Table 6.1 shows the values collected during the experiment and is used to calibrate the raw total power measurements.

Table 6.1 Total Power calibration data points

rQ Value	$X^2$	Voltage (V)	Temperature (K)
.1139		1.9846	77
.1730		2.1065	271.65

### 6.1.2 Data Analysis

To analyze the results, iPython Notebook is used to read and generate the graphs used in this thesis. This tool uses Python along with HTML and Markdown code to generate a virtual notebook for each experiment. Figure 6.1 shows a screen shot of a iPython notebook used in this thesis

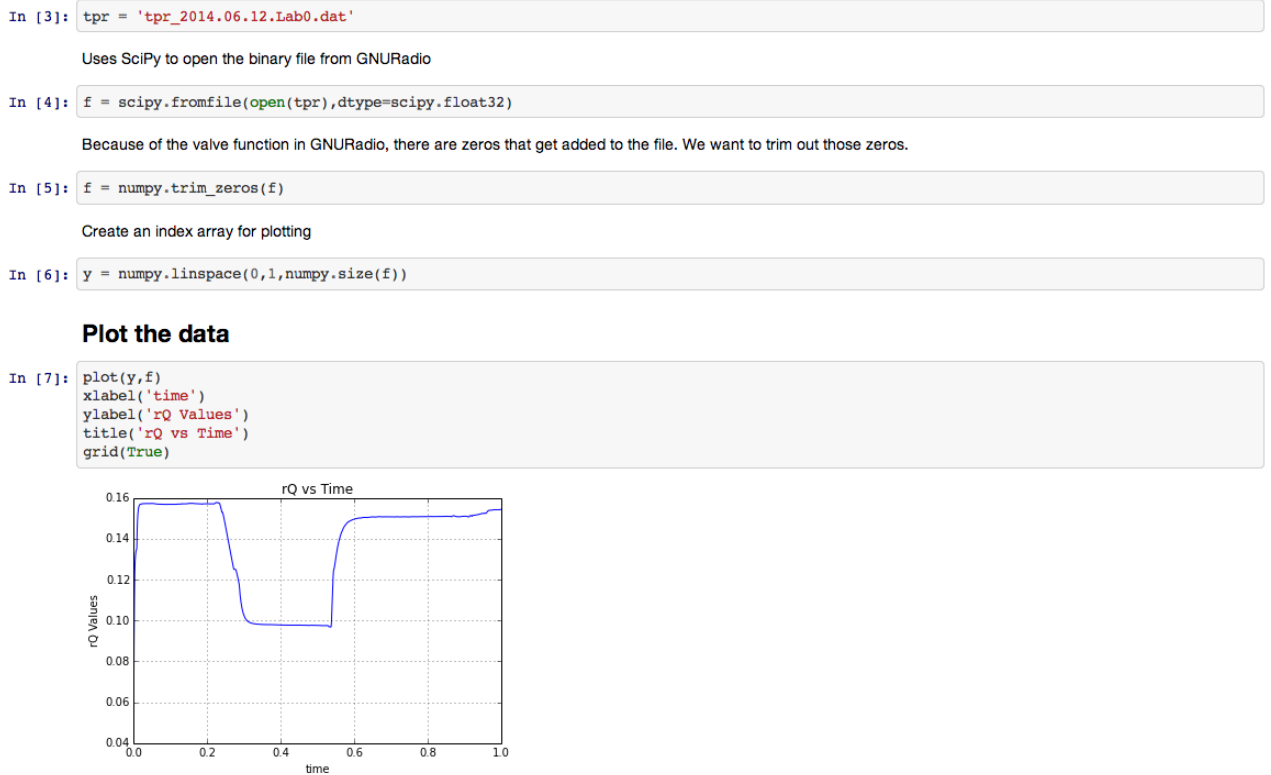


Figure 6.1 A screenshot showing the iPython notebook code and related graphs generated for parsing GNURadio data

*Software Defined Radio Data.* The SDR records the total power measurements in a binary file that either Matlab or Python can read. This file format is explained in section 5.1.2. We begin by looking at the raw or uncalibrated total power readings. This power information is information collected after the total power radio block in GNURadio and is explained in Chapter 4. Because the values are uncalibrated total power readings, there are no units.

Figure 6.2 shows the total power reading versus time. This figure has also been annotated to show which medium the matched load has been placed in (i.e. Ice water, LN2, Hot water).

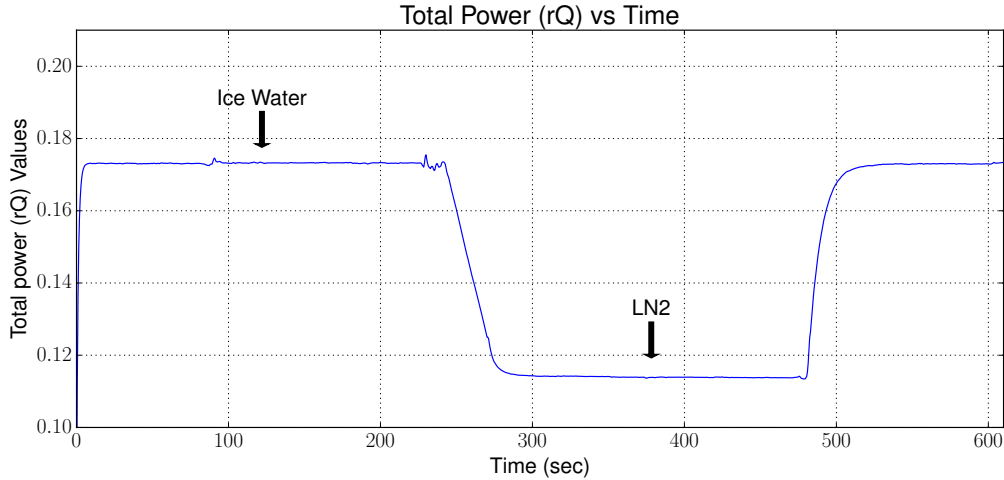


Figure 6.2 Graph of the uncalibrated SDR total power values of Experiment I

Since we know the temperatures of the ice water and LN2, we can calibrate these readings to a noise temperature reading. This is done by reading a calibration file we have stored in a csv format and solving for the slope of a line. This was accomplished using the following code written in Python.

```
a=numpy.array ([[ rQ_values [0] ,1.0],[ rQ_values [1] ,1.0]] ,numpy.float32 )
b=numpy.array ([ temp_values [0] ,temp_values [1]])
z=numpy.linalg.solve (a,b)
```

Now that we have our calibration points, we can re-graph this data as calibrated noise temperature as shown in Figure 6.3. Figure 6.3 is also colorized to represent “warmer” to “cooler” noise temperatures.

*Square Law Detector Data.* Now that we have looked at the software defined radio data, we want to examine the square-law detector data and then compare the two. The square-law detector gives us power information as a voltage. In order to compare the square-law detector to the SDR data we will also calibrate it as a noise temperature. We can do that using the same method as the SDR and calibrate the voltages to the known temperature references. It can be seen in Figure 6.4 that the data from the square-law detector is very noisy. Therefore, we use a filter to smooth out the data.

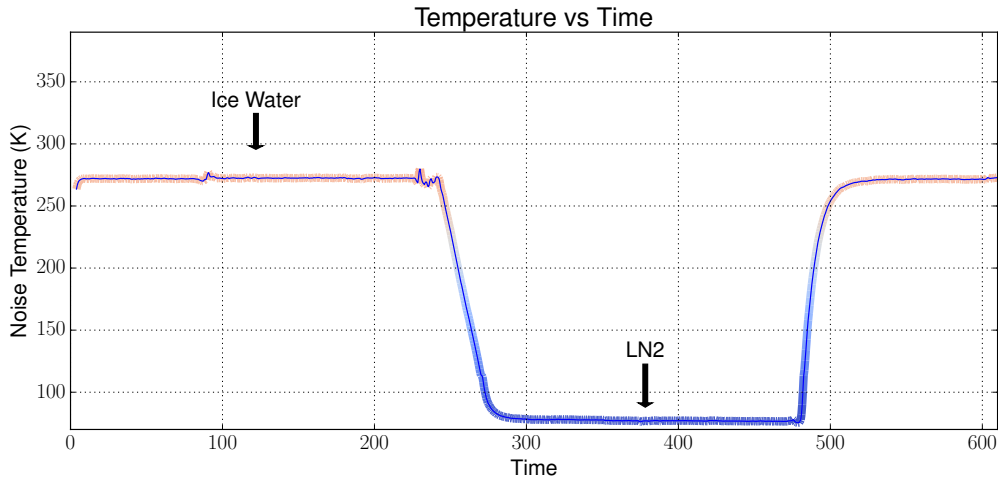


Figure 6.3 Graph of the SDR calibrated noise temperature for Experiment I

To filter the data, Python in conjunction with SciPy is used. For this experiment, we use a low pass filter to smooth out the signal. The following code applies the filter to the data.

```
from scipy import signal
N=100 # Number of taps
Fc=40 # Cutoff Frequency
Fs=1600 #Sample Frequency
h=scipy.signal.firwin(numtaps=N, cutoff=Fc, nyq=Fs/2)
x2_filt=scipy.signal.lfilter(h, 1.0, x2_voltage)
```

Figure 6.5 shows our data after being filtered by the low pass filter. Using the same technique as earlier, we can now calibrate the raw voltages from the square-law detector to the noise temperature. As with the data collected from the SDR-based radiometer, the data from the square-law detector is calibrated to the physical temperature that our matched load is placed in. Figure 6.6 shows the calibrated data from the square-law detector. This now allows us to directly compare the square-law detector to the software defined radio data since we have a common reference point.

*SDR-based radiometer vs square-law detector.* We now compare the Software Defined Radio Based Radiometer with the square-law to make sure they match. Because both the SDR-Based

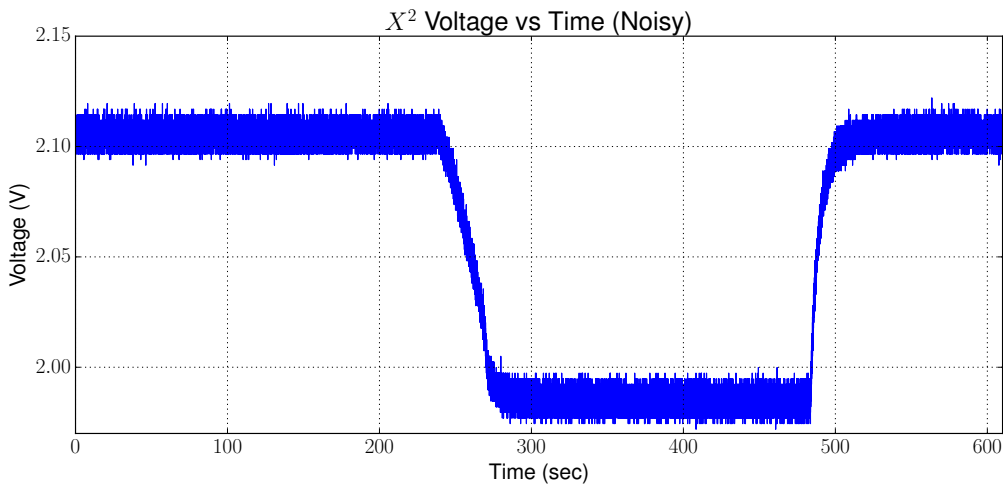


Figure 6.4 Unfiltered data from the square-law detector collected in Experiment I

Radiometer and the square-law are now calibrated to a noise temperature, we can graph both sets of data and compare them to each other.

We can see in Figure 6.7 that both the software defined radio and the square-law detector match up very nicely. This shows that both the square-law detector and the software defined radio agree when properly calibrated. This verifies that the software defined radio can indeed operate as a total power radiometer and the data we obtain from this setup agrees with an analog and more traditional radiometer.

## 6.2 Experiment II - Evaluation of sensitivity and stability

### 6.2.1 Data Collected

This experiment examines the sensitivity and stability of a SDR-based radiometer. The data used for the sensitivity is the same data collected in experiment one in section 6.1.1. The data collected for the stability is the total power data collected from the SDR-based radiometer over a period of 15 minutes. For the sensitivity data, the data is calibrated using Table 6.1. For the stability data it is calibrated using Table 6.2.

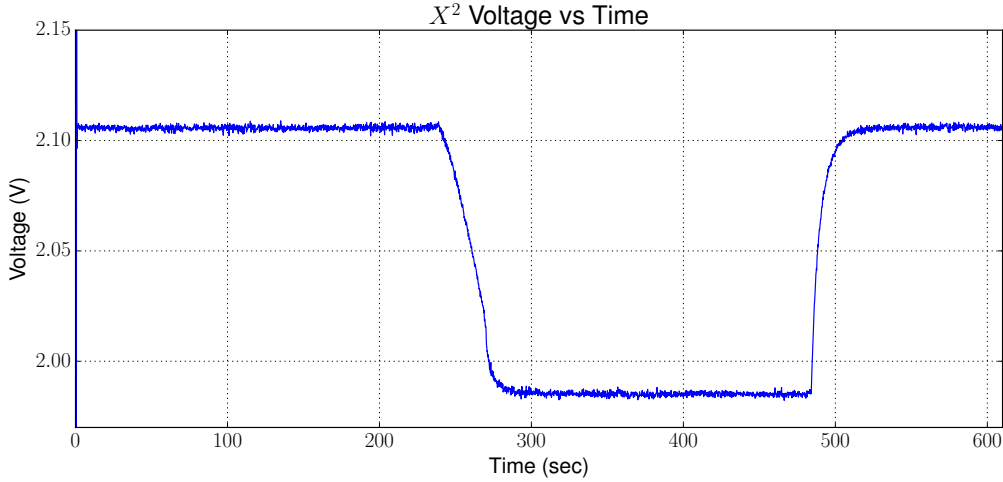


Figure 6.5 Filtered data from the square-law detector used in Experiment I

Table 6.2 Total Power calibration data points for the stability experiment

<b>rQ Value</b>	<b>Temperature (K)</b>
.1132	77
.1770	271.65

### 6.2.2 Data Analysis

*Sensitivity.* Sensitivity for a radiometer is the  $NE\Delta T$  that was covered in chapter 3 and is found in Equation 3.6. The sensitivity can also be measured as the standard deviation of the data that we collect from the software defined radiometer.

Table 6.3 Experimental parameters for experiment one.

<b>Bandwidth (<math>\beta</math>)</b>	<b>Integration Time (<math>\tau</math>)</b>	$T_A + T_N$
10 MHz	2 sec	427 K

Python is used to calculate the  $NE\Delta T$  using the data from table 6.3. The python code listed below is used to calculate the theoretical  $NE\Delta T$ .

```
tau = 2 # Integration Time
BSDR = 10e6 # Bandwidth
TN = 350 # System noise temperature
```

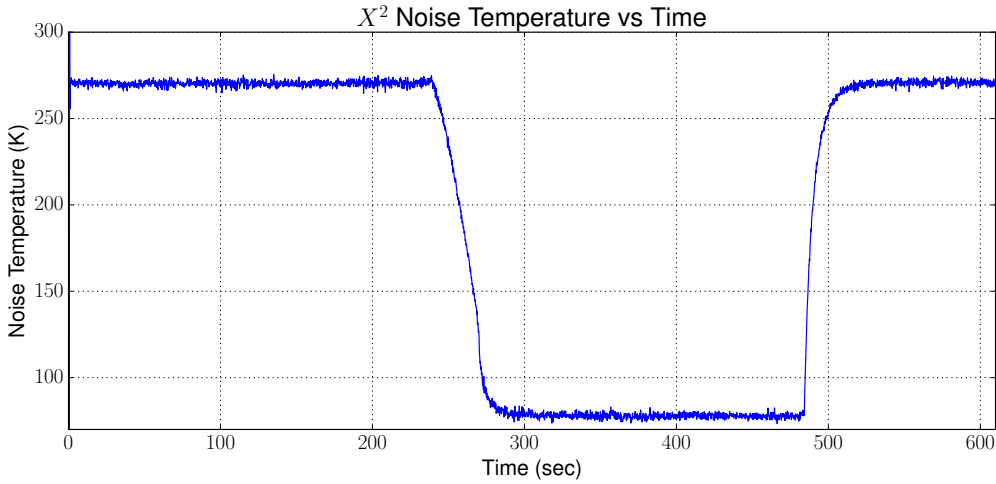


Figure 6.6 Calibrated data from the square-law detector used in Experiment I

```
TA = 77 # Antenna noise temperature
NEAT_SDR = (TA+TN) / sqrt (BSDR*tau)
```

This gives us 0.1 Kelvin for the expected  $NE\Delta T$ . Since the sensitivity is related to the standard deviation of the graph, we can use Python to give us the standard deviation of the data graphed in Figure 6.8. Figure 6.8 uses the data graphed in 6.3 but zoomed in from 350 to 450 seconds.

Python is used to determine the standard deviation of this range of data. The code used is shown below and gives a result of .23 Kelvin. We can now plot both the expected sensitivity and the actual sensitivity which is shown in Figure 6.9.

```
stdsdr = numpy.std(g)
print stdsdr
```

While .23 Kelvin is higher than the calculated sensitivity, it is still quite acceptable. As discussed in chapter 4 and shown in table 4.1, our target  $NE\Delta T$  is one Kelvin or less. Therefore our actual performance of .23 Kelvin still meets our radiometer requirement.

*Stability.* To verify stability of the radiometer, we look to see how much change the radiometer records over a relatively long period of time. To test this, a matched load was submerged

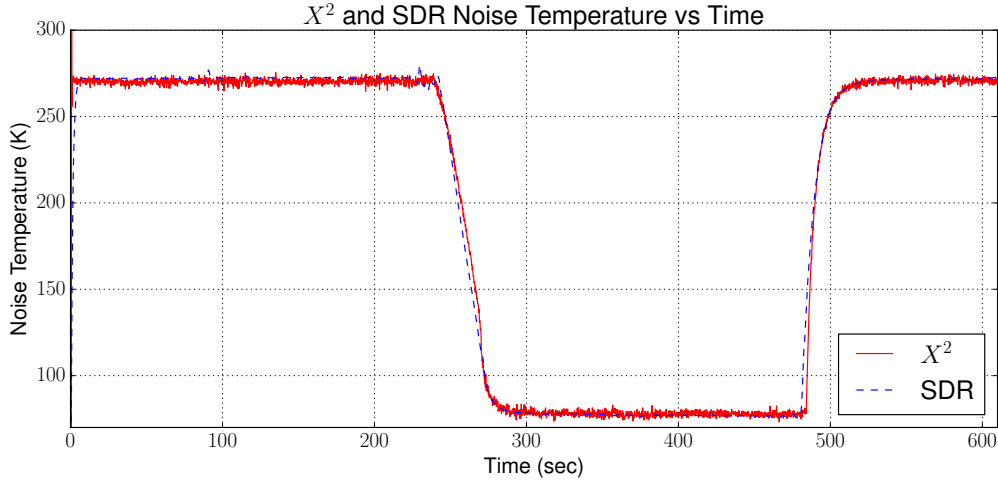


Figure 6.7 Figure showing both the SDR and square-law noise temperature data in Experiment I

in a liquid nitrogen bath for an extended period of time, in this case for fifteen minutes. The readings were then examined to study the trend of the data. The data is graphed in figure 6.10.

We can use Python to calculate a second order polynomial to create a line to fit the data in Figure 6.10. An ideal line would be flat to show no overall change with the data. In Figure 6.11 we can see that the line and the data does not change more than 0.05 Kelvin over this fifteen minute period.

### 6.3 Experiment III - Interfering Signal Mitigation

The addition of an unwanted interfering signal has an adverse effect on how a radiometer operates [Ellingson et al. (2003)]. This is a growing problem for all radiometers, but is a greater issue for radiometers used in orbiting spacecrafts to observe the Earth as they see large areas that could contain interfering signal sources [Misra et al. (2012)]. Even though the band we are working in (i.e. 1.4 GHz) is an internationally protected frequency, there have been both intentional and unintentional signal sources in this band detected by current space borne radiometers that have caused interference [Forte et al. (2013)].

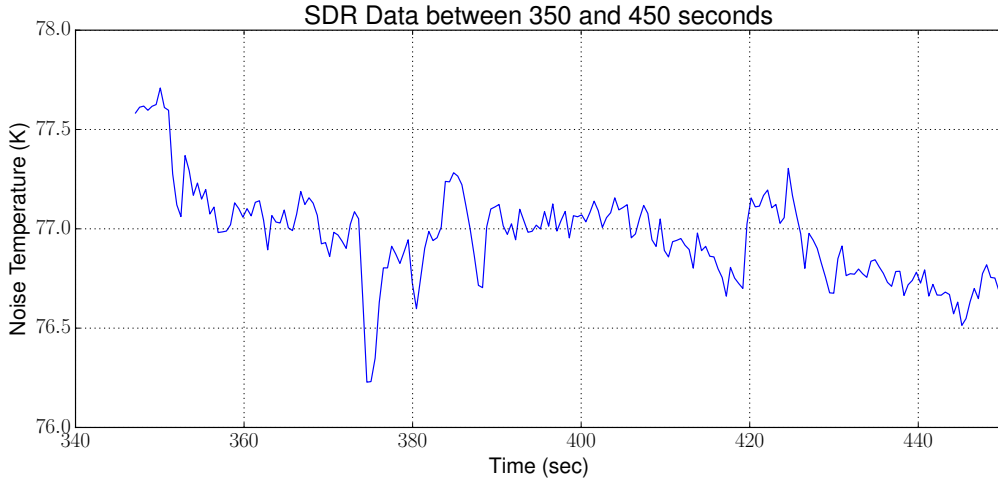


Figure 6.8 Graph of the calibrated total power from Experiment I while the matched load is submerged in LN2 between 350 and 450 seconds.

### 6.3.1 Data Collected

The data collected for Experiment III is the total power values from the SDR-based radiometer and the voltage data from the square-law detector. These values are calibrated using the data points provided in table 6.4. These values differ from the previous tables because the filter is turned on. This changes the performance of the SDR-based radiometer and results in different rQ values. The voltages are higher due to the presence of the offending signal.

Table 6.4 Total Power calibration data points

rQ Value	$X^2$	Voltage (V)	Temperature (K)
.0361		2.1234	77
.0623		2.1872	271.65

### 6.3.2 Data Analysis

We begin by looking at what happens to our total power readings when no RFI mitigation is used. As we stated in Section 5.3.1, the frequency of the offending signal will not change, but the amplitude will. This results in clear indications of the total power changing as the amplitude of the offending signal changes.

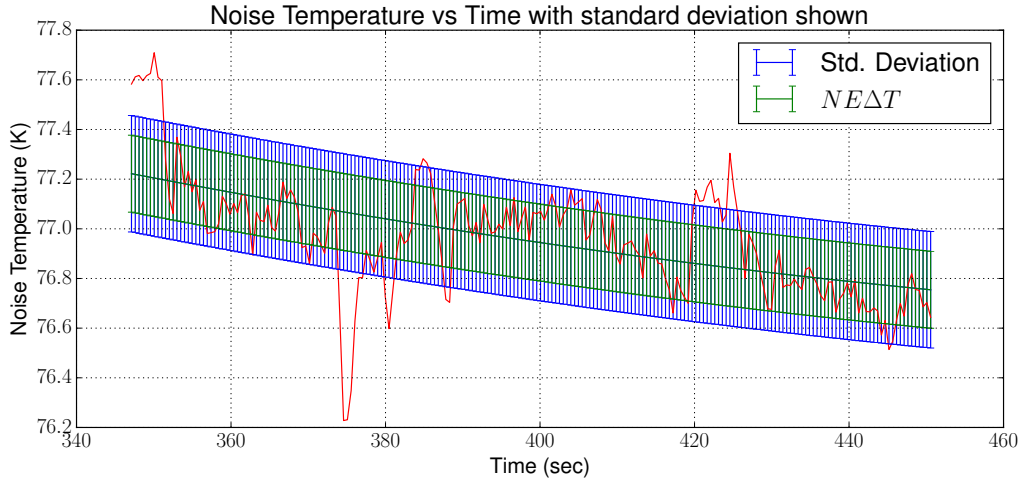


Figure 6.9 Graph of the calibrated total power with expected and actual sensitivity.

It can be seen that there are pulses that occur in Figure 6.12 that correspond to changes in the amplitude of the offending signal that affect our total power readings. These same pulses can be seen in the square-law detector data shown in Figure 6.13.

We can see in both the software defined radio and the square-law detector that there is an interfering signal. If we now look at the spectrum view of the software defined radio, shown in 6.14, we can see the signal in question occurs at 1.405 GHz. The square-law detector has no frequency information, so our only method to detect an interfering signal is by looking at the total power readings. In Figure 6.13 we can see the spikes in the square-law data, however, we do not know where in the spectrum the offending signal is located.

Since we know where the offending signal is located for the SDR-based radiometer, we can design a filter to remove this signal. In GNURadio, we can specify both the frequency and the bandwidth that we desire for this band-reject filter. Ideally we want to keep the bandwidth of the filter as tight as possible to the offending signal, while making sure our filter is effective in removing the signal. Figure 6.15 shows the spectrum display of the software defined radio while filtering the offending signal.

Since we have now removed the offending signal, we want to re-run our experiment and once again compare the difference between the software defined radio and the square law detector.

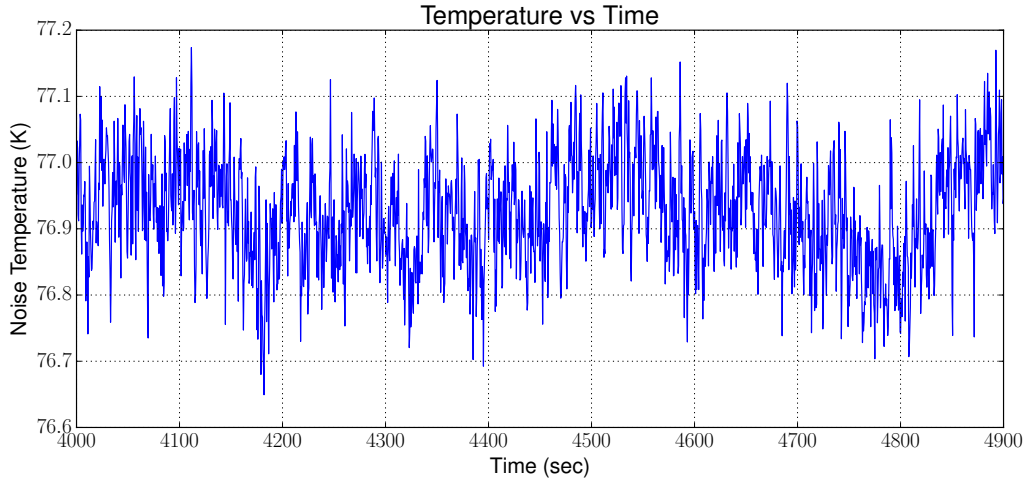


Figure 6.10 Graph of the calibrated total power over a period of fifteen minutes.

We can begin by looking at the software defined radio total power readings. Figure 6.16 shows a calibrated graph of the noise temperature seen by the software defined radio. This graph is similar to graphs we expect from a total power radiometer. However, we want to compare this to our square-law detector as well.

Figure 6.17 shows both the software defined radio and the square-law detector calibrated total power readings. In this graph you can see that the software defined radio is able to make normal readings where the square-law detector still shows changes in amplitude corresponding to offending signal pulses, which would make both calibration and obtaining useful data difficult.

*Filter delay.* It should be noted that when doing data analysis, that there will be some delay due to two factors. First, there is a delay in the software defined radiometer due to the integrator that is used. This creates a time delay as the integrator accumulates information and then settles. We use fairly large integration times, usually in seconds so this can add a significant delay. Second we do have a smaller delay in the decimation and low pass filter also used in the software defined radiometer. These are Finite Impulse Response (FIR) filters and thus have a delay given in equation 6.1, where  $N$  is the number of taps generated and  $F_s$  is our sampling frequency, in our case 10 MHz.

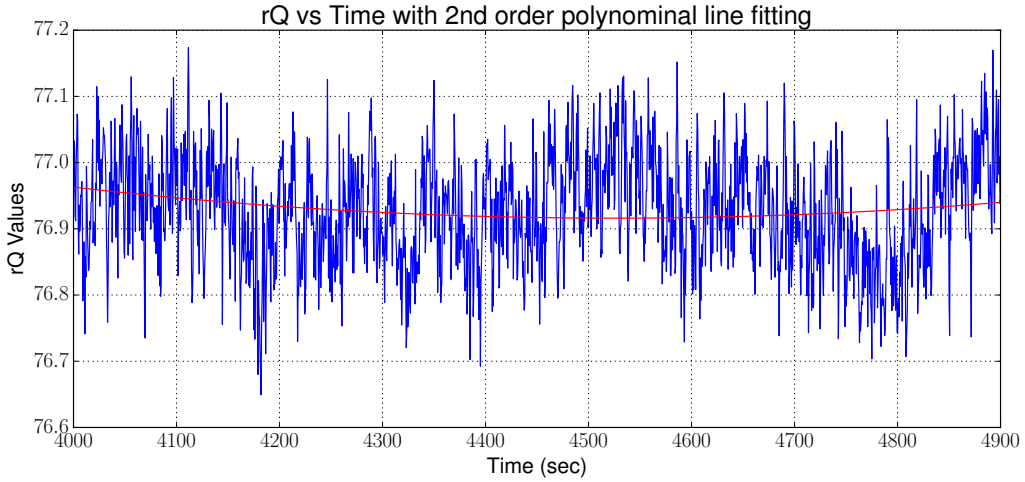


Figure 6.11 Graph of the calibrated total power over a period of 15 minutes with a best fitted line.

$$\frac{(N - 1)}{(2 * F_s)} \quad (6.1)$$

The taps value is generated by Python using the filter design program. For this experiment, the taps generated was 18,181. Taking this and our sampling rate into account, our FIR filter only delays the signal by 9 milliseconds.

A final note on aligning the square-law detector and the software defined radiometer data. Both systems have a record function and must be started manually by the user. They also run on separate computers. Therefore, there is a human error that also gets introduced to the system as well. This is usually no more than 1 or 2 seconds. But in this experiment it was noted that there was a slightly longer delay between the two of about 4 seconds.

#### 6.4 Experiment IV - Performance impact of interfering signal mitigation

The goal of this experiment is to examine what affect adding a filter was on the performance of the radiometer. While we have demonstrated we can filter an offending signal, this comes at a cost. This experiment examines the impact filtering out bands has on the measurement of total power and radiometer sensitivity.

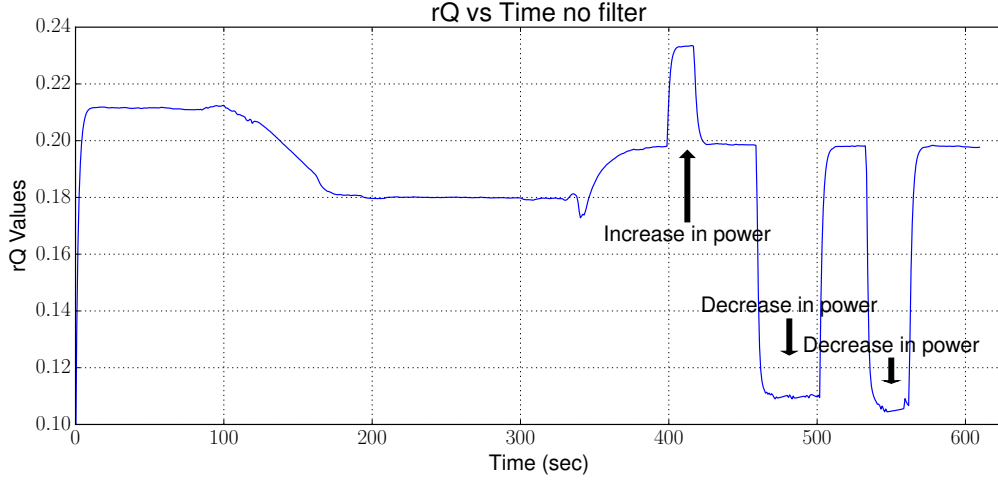


Figure 6.12 Graph showing the unfiltered total power measurements of the software defined radio

#### 6.4.1 Data Collected

The data collected for this experiment is shown tables 6.5 and 6.6, and the remaining data is data generated from Equations 6.2 and 6.3. This data will be examined next.

#### 6.4.2 Data Analysis

In Experiment IV, we examine the performance of a software defined radiometer when a filter is used. Recalling the equation for  $NE\Delta T$  from equation 3.6, our sensitivity is a function of the amount of noise from both the antenna ( $T_A$ ) and the addition of system noise ( $T_N$ ). Sensitivity is also a function of the radiometer's bandwidth ( $\beta$ ) and integration time ( $\tau$ ).

Our integration time is controllable, and can be set using the GUI panel of the software defined radio. In a typical radiometer, we often do not have any control of the bandwidth. It is often set by the mechanical band-pass filters that are in place and the square-law detector circuit to measure the noise power. In a SDR radio, we have more control over bandwidth as we can change our sampling rate which in turns controls our bandwidth. There is a limit as larger sampling rates require higher performance ADCs and greater computing speed.

Recall from Experiment III, in section 6.3, where we filtered out an offending signal. While

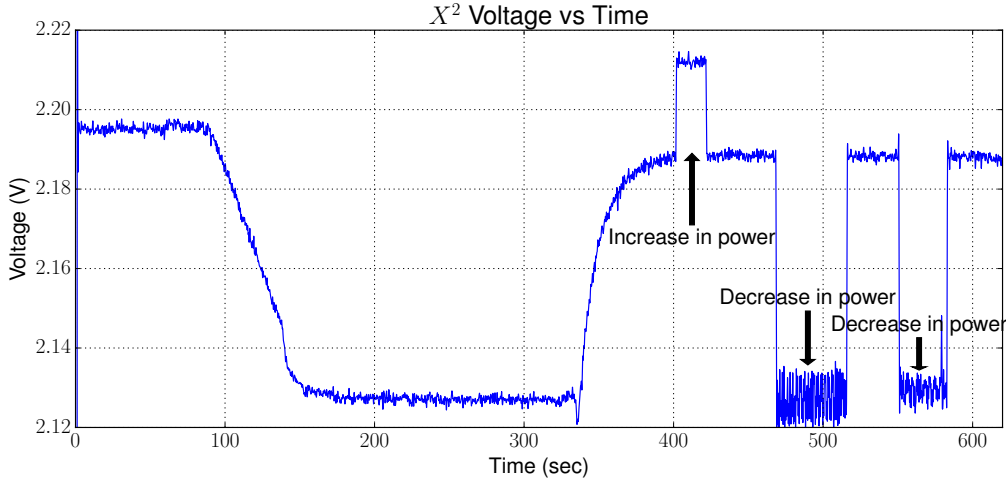


Figure 6.13 Graph showing the raw total power read from the square-law detector with an interfering signal.

we were able to filter out the offending signal and resume total power measurements, it comes at the cost of reducing the overall bandwidth available for power detection. In this experiment, we examine how this impacts sensitivity and derive the following Equation 6.2.

$$NE\Delta T = \frac{T_A + T_N}{\sqrt{(\beta - \beta_{filter})\tau}} \quad (6.2)$$

Because we are notching out a portion of the bandwidth in order to remove the offending signal, this also removes that bandwidth for total power detection. As the bandwidth of the filter ( $\beta_{filter}$ ) increases, the more bandwidth that is subtracted from the total bandwidth ( $\beta$ ) available. Equation 6.2 accounts for this loss by subtracting the filter bandwidth ( $\beta_{filter}$ ) from the total bandwidth ( $\beta$ ).

We can graph the expected response of the  $NE\Delta T$  by adjusting the values of  $\beta_{filter}$  to range from a narrow-band filter, in our example 125 kHz, all the way to 9.99 MHz or nearly all of the bandwidth. Figure 6.18 shows the expected exponential response of  $NE\Delta T$  as the size of the filter increases.

Figure 6.18 shows measured standard deviation points for the SDR-based radiometer for different filter sizes. These filter sizes and collected data found is found in table 6.5. It can

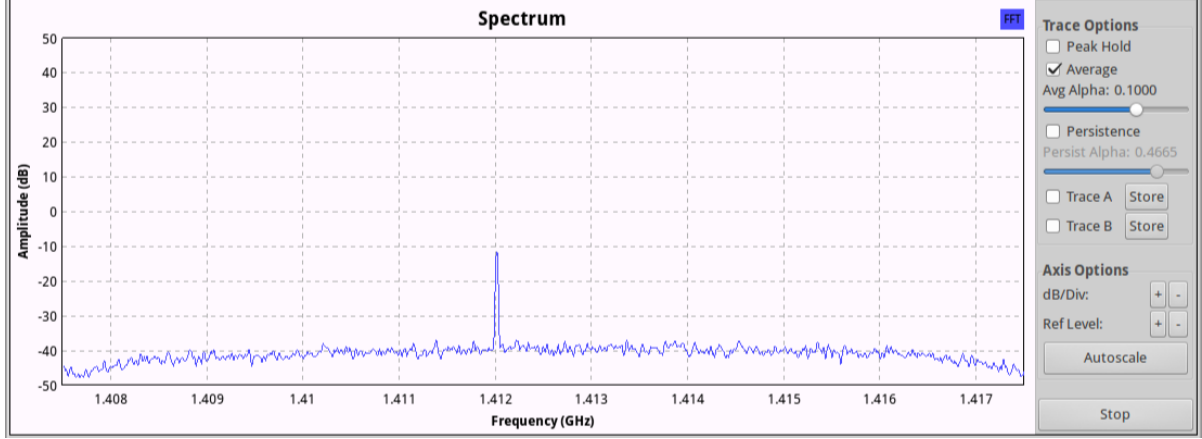


Figure 6.14 Image showing the spectrum view of the SDR-based radiometer with no RFI mitigation.

be seen in figure 6.18 that there is a good correlation between the expected sensitivity of the radiometer and the measured sensitivity of the radiometer.

Finally a line is added to figure 6.18 to show a possible limit of when we may have filtered too much. In this example a  $NE\Delta T$  of 0.2 Kelvin is used. In figure 6.18 it can be seen that at about 5 MHz, our  $NE\Delta T$  exceeds our threshold of 0.2 Kelvin. This would mean that to meet this performance criteria we would need to not exceed 5 MHz for our filter size. This is assuming our integration time ( $\tau$ ) and the bandwidth ( $\beta$ ) is held constant.

We now look at the relationship of the total power received as the bandwidth decreases. Figure 6.19 shows both the measured total power received and the expected total power received as the bandwidth of the filter increases.

The total power is calculated from equation 3.2 and is based on the system noise ( $T_N$ ), and the antenna ( $T_A$ ), the bandwidth ( $\beta$ ) and the gain ( $G$ ) of the amplifiers used. Our gain and noise temperatures are fixed, and in this experiment we use a system gain of 30 dB. This represents the gain that we see with the three LNAs used minus any losses or attenuation placed in the RF chain. What changes in this experiment is the amount of bandwidth. Again, we can modify equation 3.2 by subtracting the filter bandwidth ( $\beta_{filter}$ ) from the total bandwidth available and is shown in equation 6.3.

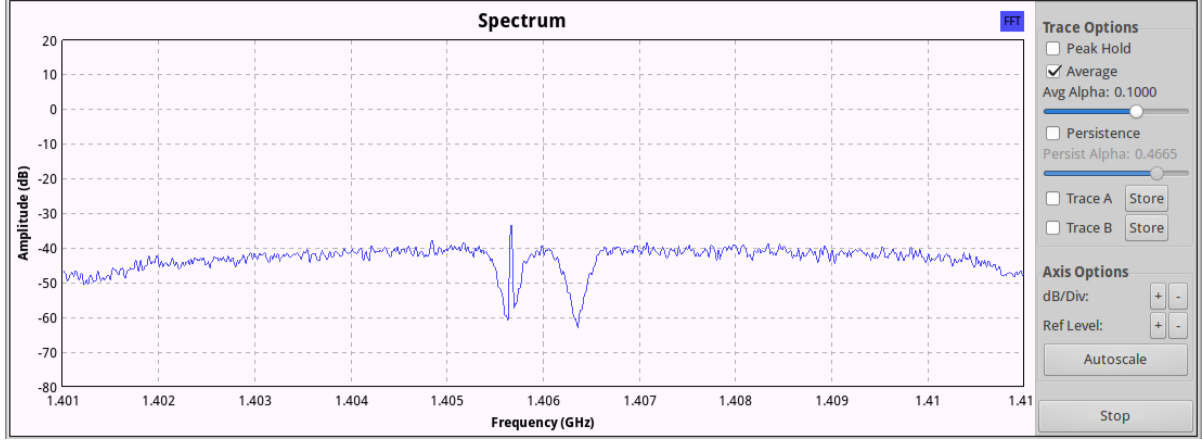


Figure 6.15 Image showing the spectrum view from the SDR-based radiometer filtering the offending signal

$$P_{out} = k(\beta - \beta_{filter})G(T_A + T_N) \quad (6.3)$$

To compare this theoretical power to the actual power measured, we collected the rQ values by once again creating different filter sizes and then measuring the rQ values. These values can be found in Table 6.6 and are added as dots to Figure 6.19. This also shows a very good correlation between the expected total power received and the measured total power received for Experiment IV.

#### 6.4.3 Usage Scenario

*Application with Soil Moisture Readings.* A common application of radiometers is in the measurement of soil moisture. All items naturally emit RF energy due to the random excitation by the electrons in the object. The amount of noise that gets generated varies by temperature and the amount that reaches the antenna varies by the amount of moisture in the soil. If we calibrate the radiometer to two known soil conditions, then we can measure the various levels of soil moisture in the soil. We will assume the soil is at a constant temperature during the observation. We will look at the percentage of moisture in the soil, which will vary from zero percent or dry soil to one hundred percent or very wet soil. The drier the soil, the more

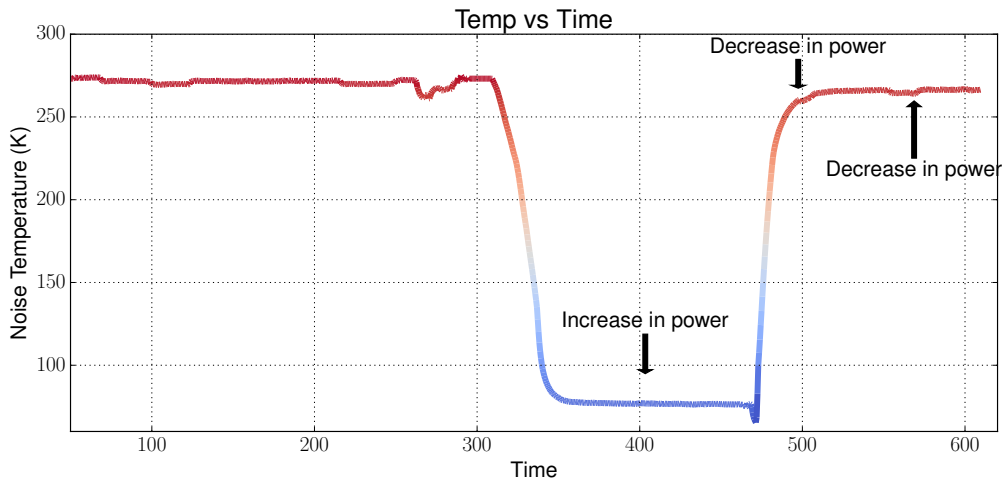


Figure 6.16 Graph showing the calibrated total power readings with the filter removing the offending signal

thermal noise we receive and the "warmer" the noise temperature. Wet soil on the other hand attenuates the thermal noise and shows up as a "cooler" noise temperature.

Using the SDR-based radiometer, we can set up two methods to visually look at the noise temperature and thus the soil moisture percentage. Since we do not have an antenna hooked up, we will simulate this by using a matched load submerged in two reference temperatures. In this case the ice water bath and the LN2 bath that was shown earlier.

A unique visual aid we can use with GNURadio is a waterfall display. This display gives us information that includes frequency, amplitude and time. It is referred to as a waterfall display due to the fact the display continually moves from top to bottom and looks like a waterfall. Amplitude information is given by mapping the range of amplitudes to a color bar. Frequency is given on the x-axis and time is on the y-axis. Figure 6.20 shows a screen shot of the waterfall display in the GUI created in GNURadio Companion for this experiment. This is the same program we have used but with the waterfall display now added. The data for the waterfall is pulled directly from our source block or in our case the N200 software defined radio.

Two screen shots of the waterfall side by side is shown in Figure 6.21. The left image shows the matched load in Ice Water and the right image shows it in LN2.

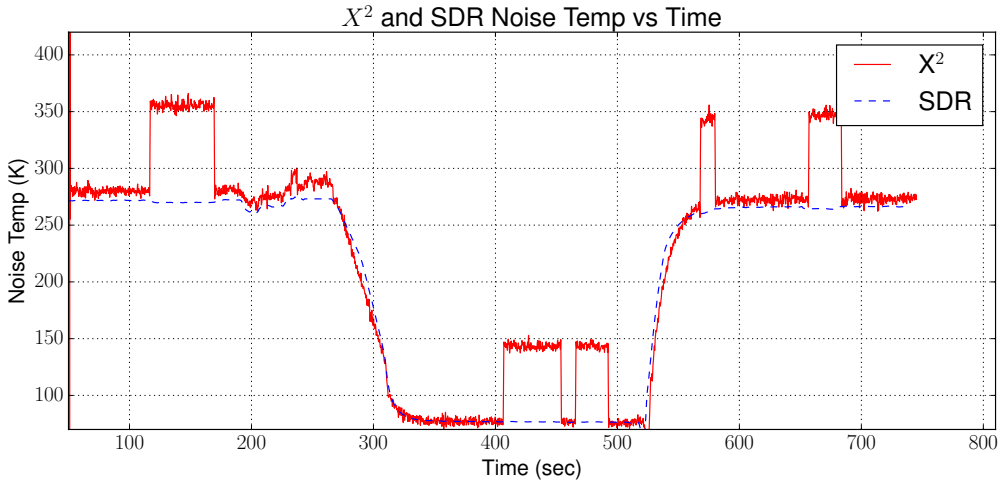


Figure 6.17 Image of the offending signal being filtered out by the SDR. It can be seen that the signal is no longer visible.

Figure 6.21 we can see that the ice water screen shot (on the left) appears warmer than the right side screen shot which appears cooler. There is a limitation in GNURadio and the waterfall display that limits what the range for the power readings are. The overall power that we see only changes by about 3 dB and our current range in the waterfall display is set to 10 dB. If we could reduce the range, the color change would be even greater and more pronounced. However, this does show that a change can be seen visually with color to indicate the noise temperature.

If we assume that our LN2 is dry soil and that our ice water bath is wet soil, we can now interpolate the data to this scale and show the information we obtained in Experiment one as both a noise temperature and soil moisture. Figure 6.22 shows the data shown in Figure 6.3 but with the soil moisture percentage added.

While this demonstrates that we can calibrate our total power readings with a soil moisture percentage, we would use actual field tests to calibrate the radiometer. In addition, we could also calibrate to soil moisture content instead of a percentage if desired. Both methods have been done with traditional radiometers[Jonard et al. (2011)][Shi et al. (2003)].

*Mitigating interference.* Experiment III demonstrates that an offending signal will impact

Table 6.5 Measured sensitivity and Bandwidth of Filter

NEAT (K)	Bandwidth (MHz)
.139	.125
.141	.250
.143	.500
.147	1
.153	2
.166	3
.181	4
.195	5
.234	6
.252	7
.318	8
.450	9
1.45	10

and cause the total power received to increase. This increase in total power will then invalidate our calibration of the SDR-based radiometer. This will result in a spike as shown in Figure 6.12. This spike shows a higher than normal total power which will result in a higher noise temperature. A higher noise temperature will then cause the SDR-based radiometer to show drier soil conditions than what is actually present.

By mitigating the interfering signal the SDR-based radiometer is able to make calibrated soil moisture measurements even with the signal present. Figure 6.16 demonstrates the SDR-based radiometer making total power measurements with an offending signal present.

Soil moisture measurements can continue with an offending signal present, however there is an impact on the system with filtering out this signal. This is covered in Section 6.4. Because of this impact, re-calibration of the SDR-based radiometer still needs to take place. Therefore while this solution is viable for interfering signals that are constant, other methods would need to be developed to handle sporadic interference.

## 6.5 Advantages of a Software Defined Radio Based Radiometer

A study was conducted on what benefits a software defined radio radiometer would have over a more traditional radiometer. We focused on three main areas; cost, weight and size, and

Table 6.6 Measured Total Power and Bandwidth of Signal

Total Power Value (rQ)	Bandwidth (MHz)
.003	.125
.006	.250
.012	.500
.025	1
.050	2
.071	3
.101	4
.125	5
.140	6
.170	7
.200	8
.230	9
.250	10

the value a SDR-based radiometer can add over traditional radiometers.

### 6.5.1 Cost Benefits

Software defined radios have become more commonplace in recent years and this has generated a number of Commercial Off The Shelf (COTS) solutions. A COTS solution is often a lower cost solution due to the mass manufacturing that takes place. This has driven the cost of many SDRs to under one thousand dollars, while still having excellent performance characteristics. The N200 SDR purchased for this research cost fifteen hundred dollars and the daughter-board approximately cost one hundred and fifty dollars. Other software defined radios however have come out on the market since then. Ettus, for example, has some that are below one thousand dollars and the author has also obtained the HackRF One SDR that now sells for three hundred dollars. The main difference between defined radios on the market is in their resolution and the bandwidth they support.

As seen in table 6.7, even the higher cost Ettus research equipment is a lower cost option than the custom built radiometer in use at Iowa State University, and even a comparable off the shelf radiometer. It should be noted that the radiometer in use at Iowa State University is also a dual polarization radiometer so there are two RF front ends and two ADCs that feed

---

<sup>1</sup>Purchase price in 2005

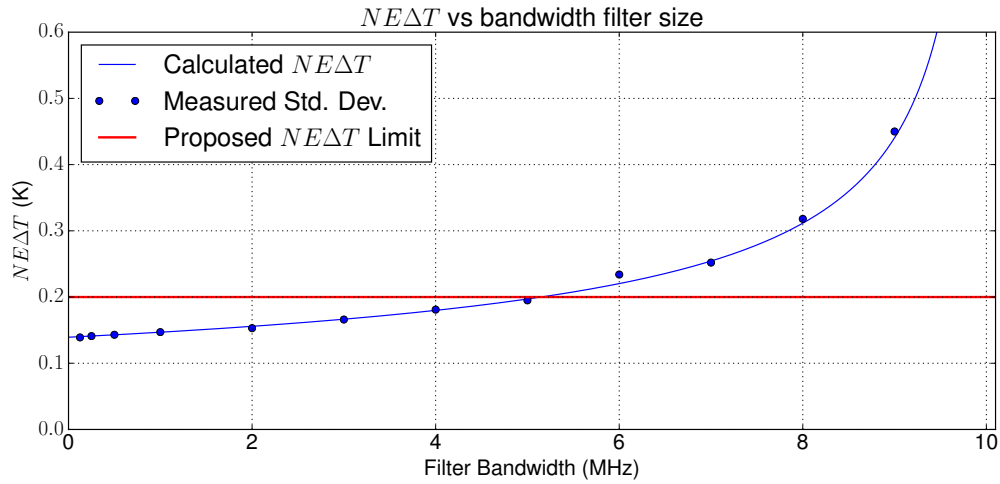


Figure 6.18 Graph of the calculated  $NE\Delta T$ , the proposed limit for the sensitivity of the radiometer, and the measured standard deviation with respect to filter bandwidth.

into a FPGA board. It would be quite easy to add dual polarization to the Ettus N200 SDR as it does support two daughter-boards. This would increase the cost to \$2,179 for the additional LNAs and daughter-board.

The largest cost benefit is that key components that you find in a radiometer, the filters and square-law detector, can be performed in software instead of needing additional equipment. The system is also much more frequency agile, which means it can work over a broader range of frequencies than most traditional radiometers, with very little change in hardware and in

Table 6.7 Cost Analysis

Device	Quantity	Cost
<b>SDR Solution</b>		
N200 SDR	1	\$1515
LNA at \$60 ea.	3	\$180
DBSRX2 Daughter-board	1	\$152
GNURadio	1	\$0
Total		\$1847
<b>ISU Radiometer</b>		
LNA, FPGA, ADC, Microcontroller and power supplies	1	\$10,000 <sup>1</sup>
<b>Commercial Off the Shelf Unit</b>		
Spectracyber 1420 MHz Hydrogen Line Spectrometer	1	\$2,650

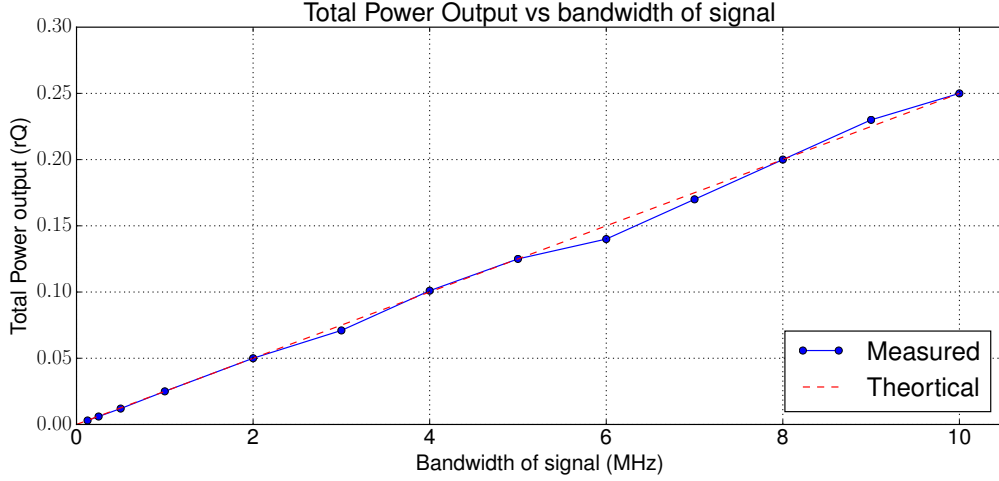


Figure 6.19 Graph of the total power measured and theoretical power versus the bandwidth of the measured signal.

some cases may require no change in hardware. The Ettus N200, for example, uses daughter-boards to provide the RF interface. While these boards provide a high quality RF signal, it does come at a cost and are usually designed for certain bands of frequencies. Other low cost SDRs, however, also support a wide range of frequencies. The HackRF, for example, works from 10 MHz to 6 GHz, but does so at the cost of lower resolution, less gain in its front-end, and supports a lower bandwidth.

### 6.5.2 Weight and component size benefits

A typical radiometer has many components that are involved in its design. This includes filters, LNAs, and the power detection (i.e. square-law detector) used. These components add weight, size and costs to a radiometer. A software defined radio however digitizes the signal and we are able to replace the filters and square-law detector with their software equivalent. While a software defined radio does add an ADC and usually a FPGA to perform signal processing, advances in semiconductor technology has continued to shrink these components. These components are also lighter than the filters often used in traditional radiometers. Table 6.8 displays the mass for the SDR-based radiometer built and the ISU Radiometer. The ISU

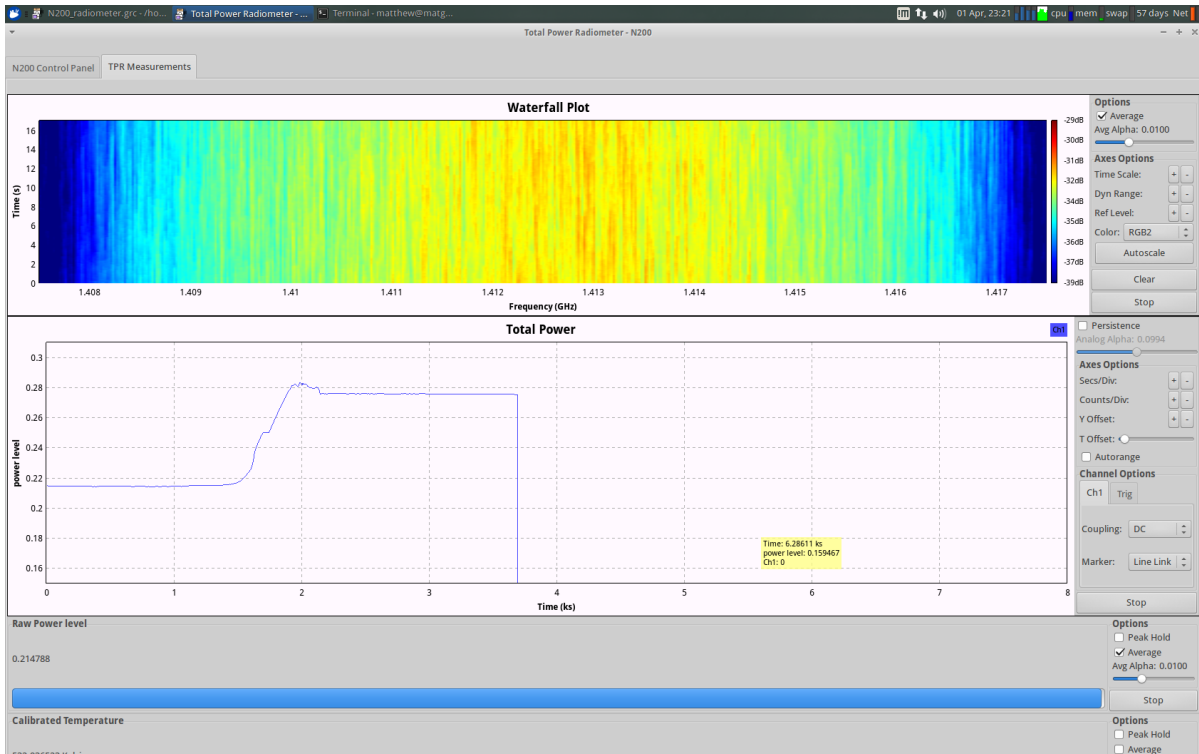


Figure 6.20 Screenshot of the waterfall display showing the magnitude of the received power as a color, the frequency on the y-axis and time on the x-axis.

Radiometer is a representation of most traditional radiometers.

Size is another benefit, since semiconductor technology has continued to shrink components. Again, since items like the filters and square-law detector are replaced with software implementations, this helps to reduce the overall size.

### 6.5.3 Value added benefits

A SDR-based radiometer adds additional value for two reasons. One, it is able to work with both frequency and magnitude information, where a traditional radiometer does not. This allows for additional analysis on the signal and can help identify issues such as an interfering signal that was demonstrated in this thesis.

Second, we are able to have an agile system that is able to adapt to changing conditions with very little or no change to hardware. Different types of radiometers can be implemented

---

<sup>2</sup>Estimated, no data available



Figure 6.21 Side by side comparison of the waterfall display for when the matched load is submerged in LN2 and ice water.

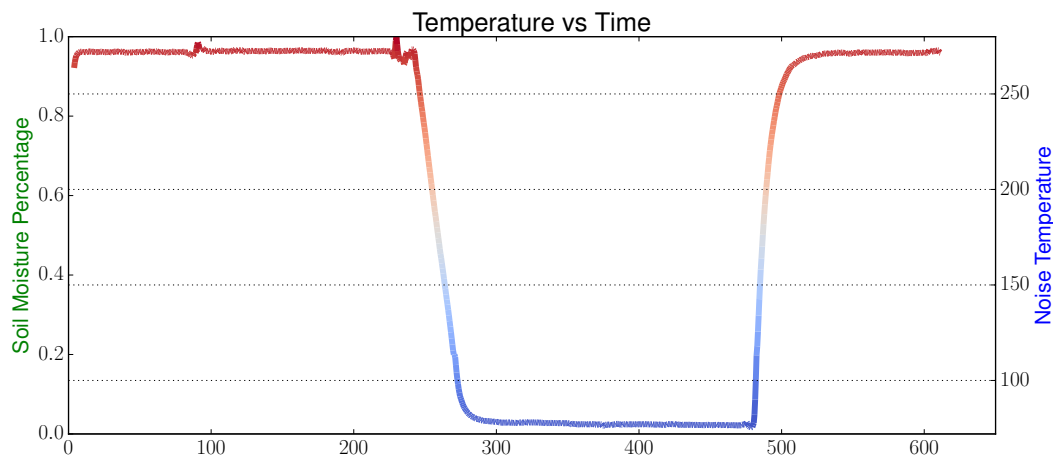


Figure 6.22 Plot of the noise temperature of Experiment 1 with soil moisture percentage

such as a Dicke radiometer, dual polarization radiometer, or a radiometer that can perform Stokes parameters. In addition, since we have both frequency and power information, we can create a system that is able to adapt to changing conditions, such as dealing with an interfering signal.

## 6.6 Drawbacks of a SDR-based Radiometer

Although we have outlined a number of advantages of using a COTS SDR-based Radiometer and how a SDR can add additional value to the radiometer system, there are some disadvantages to a SDR-based Radiometer.

Table 6.8 Weight Analysis

Device	Mass
<b>SDR Solution</b>	
N200 SDR	1.2 kg
LNA at .03 kg ea	.09 kg
DBSRX2 Daughter-board	.1 kg
Total	1.39 kg
<b>ISU Radiometer</b>	
LNA, FPGA, ADC, Microcontroller and power supplies	22.7 kg
<b>Commercial Off the Shelf Unit</b>	
Spectracyber 1420 MHz Hydrogen Line Spectrometer	6 kg <sup>2</sup>

### 6.6.1 Power Consumption

One of the largest drawbacks to a SDR-based radiometer can be in the power consumption of the SDR. With the move to perform functions such as power detection and filtering we now require additional computational power to perform these tasks. With those computational cycles additional power is now required. The use of FPGAs and SoC can help to minimize these power concerns as they are more efficient than using a PC.

Power and CPU requirements also increase as we add additional functionality such as filtering an offending signal. While these additions may not require additional hardware, it can require additional processor and memory requirements. An increase and processing requirements will also increase power requirements and can also add additional requirements in cooling.

### 6.6.2 Bandwidth constraints

While SDR technology has advanced, bandwidth is still a constraint that affects SDRs and in turn a SDR-based Radiometer. Bandwidth plays a critical role in a radiometer's sensitivity as explained in this thesis, therefore the fact that many SDRs are limited in bandwidth does create a disadvantage. In many cases, this bottleneck takes place in both the transport and processing of large bandwidth systems. This also relates to the power consumption disadvantage since larger bandwidth also means requiring additional computational cycles.

In contrast, a square-law detector usually has a very large bandwidth, as much as one

gigahertz, and is why we usually need to filter to the frequency band of interest.

## CHAPTER 7. CONCLUSION AND FUTURE WORK

### 7.1 Conclusion

In this thesis we have shown that an off the shelf SDR can be used to perform as a radiometer. Using a SDR has several advantages such as a more flexible system and can result in a less expensive system by using commercial off the shelf components. Since a SDR offers high flexibility, changes to the system can be done very quickly and helps in future proofing the system.

### 7.2 Future work

The work in this thesis demonstrated a basic radiometer system. There are other more complex radiometer systems that can be implemented in software. These include a correlating radiometer or a Dicke radiometer that can improve stability of the radiometer without the need of additional equipment such as thermal electric coolers.

#### 7.2.1 Improvements

Several improvements can be done to further enhance this software defined radiometer. One improvement is to remove the personal computer (PC) and move the software defined radio to a Field Programmable Gate Array (FPGA) or an Application Specific Integrated Circuit (ASIC) solution. A second improvement is to reduce the dependency on stable Low Noise Amplifiers (LNAs) by being able to compensate for instabilities in the system.

*Removing the PC.* For this thesis we focused on the software that would run on a PC or comparable computer system running a full operating system like Linux. This aids speeding up development by using software tools such as GNURadio to rapidly develop the software

used to create a radiometer in software. While this works just fine for testing the theory on an off the shelf SDR acting as a radiometer, it does require hardware that is capable of running a full operating system and the associated software. For some applications of a radiometer, this is not a huge concern. In the case for the ISU radiometer, the concern is not that large since the radiometer is not designed to be portable and requires additional support equipment such as a generator anyway. However, other remote sensing applications, such as space based applications, would require a more efficient method. It is very possible to move the software generated in GNURadio into the firmware of the N200. This will help to offload the work needed by the computer and would allow for the computer or similar system to act as more of a control method and for data storage.

*Improving stability.* One of the largest challenges with a radiometer is improving the stability of the radiometer. Drifts in temperature can greatly affect the gains from the LNAs and also change how much noise all components in the radiometer contribute. A software defined radio can help as we are digitizing the signal as soon as possible. This helps in eliminating the analog components for power detection and even for filtering, but does not eliminate all physical hardware, mainly the LNAs. In this thesis, we did not focus on this issue since the tests were done in a controlled lab environment.

However, a more compact, lower cost and easier setup would be to just have the LNAs attach directly to the SDR without any temperature compensation. While this can be done, we have now lost stability in the LNAs and we need to compensate for that. Several methods have been discussed to handle instability in a traditional radiometer. Some of these methods would be suitable for implementation in a software defined radiometer.

A very traditional method is a Dicke radiometer. A Dicke radiometer switches between the antenna and a known noise source. A future work for a software defined radiometer would be to use a digitally generated noise source, such as a Gaussian noise source, and then switch between the antenna and this known noise source. This noise source can also be adjusted and is performed in software, therefore stability in the noise source is not an issue.

*Correlation.* Another method to improve stability and sensitivity is to correlate the information with another input which can be another antenna looking at the same source or can

be two polarization from the same antenna[Clapp and Maxwell (1967)]. This results in two receiver systems looking at the same source and you have two signals,  $S_1$  and  $S_2$ . Since we are looking at the same source, both signals will be correlated in time, and when multiplied they will provide an output proportional to the strength of the source signal. The noise introduced by each receiver will then have a lower correlation due to the random nature of the noise. This results in a radiometer with a greater sensitivity due to the reduction of the noise even though two receivers are used [Fujimoto (1964)].

The N200 software defined radio was chosen as it is capable of having two different daughter-cards plugged in. Therefore, it is possible to have both sources enter the software defined radio and once digitized we can sum the magnitudes of the two incoming sources. This is quite easy to do and is shown in figure 7.1.

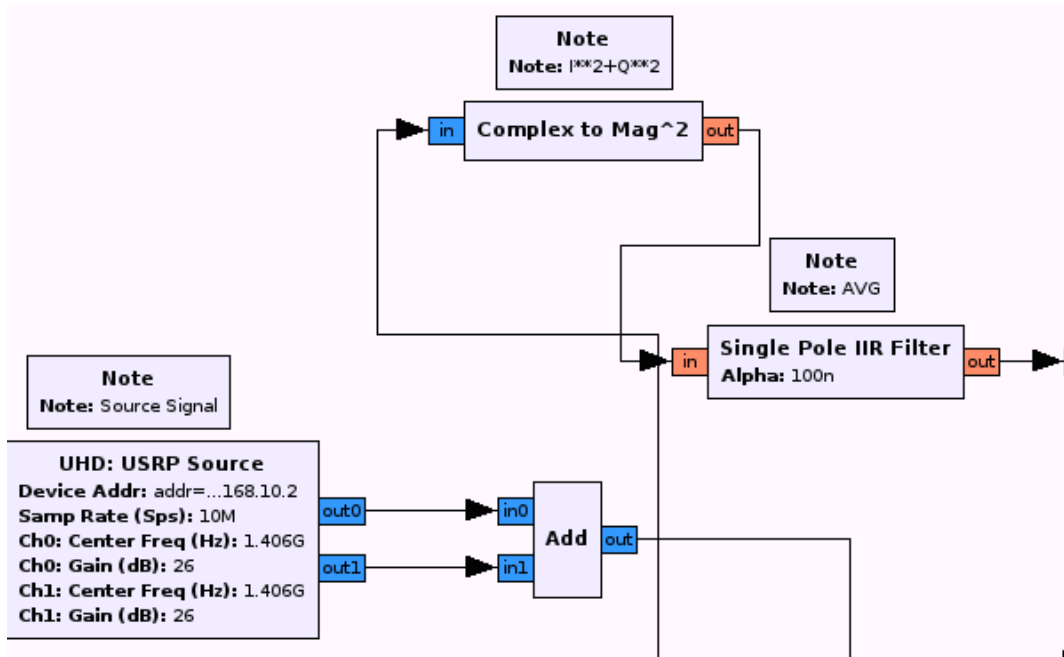


Figure 7.1 The key blocks used for creating a correlating radiometer in software. The key blocks is the USRP source, which allows us to address both daughter-boards and the ADD block which sums the signals.

Although figure 7.1 shows a correlating software defined radio radiometer, it has not been tested. In theory, this should correlate the signal and improve the sensitivity of the radiometer, however further testing is needed.

Correlation allows for unique ways for applications in radiometers including also performing beam steering [Villarino et al. (2002)]

### 7.2.2 Further testing

The improvements and additional features outlined in Section 7.2 will require additional testing and verification. While it has been shown that a software defined radiometer operates identically to a traditional radiometer, further testing is needed to verify different operating modes of a software defined radiometer.

## 7.3 Closing statement

This thesis demonstrated that it is possible to use off the shelf components and a software defined radio to implement a working radiometer that can be used in various radiometer applications such as soil moisture, ocean salinity and radio astronomy. Use of a software defined radiometer can potentially allow radiometers to be used by a wider audience of users by creating an easy to user GUI and reducing the cost and hardware complexity that most radiometers require. The result is more locations that are able to use radiometers as remote sensing tools to learn more about our planet and even the cosmos.

## APPENDIX A. Source code

The following is the source code to several programs that make the radiometer possible. The first is the Python code used with the Ettus N200 software defined radio. This code is a heir block, which means it can be imported into GNURadio and used as a block. Once imported you may run your source into this block and use any sink needed to either display or log the data. This code was generated using GNURadio Companion.

The third code supplied is Python code that can be used to read the data generated and plot it. In many ways it mimics the functions of the Matlab script buy uses Python, NumPy and SciPy to perform the mathematical functions. This may be a better option for those that wish to look at the data but do not have access to Matlab since Python is free to download.

Finally, this code has been included in this thesis as a point of reference. It may be out of date and some other pieces of code was also used for the experimentation used in this thesis. Copies of this thesis source L<sup>A</sup>T<sub>E</sub>Xcode, some experimental data, and any other code used can be found on the author's GitHub repository, <https://github.com/matgyver/Radiometer-SDR-Thesis>.

### Python code for total power radiometer

The main code that acts as the total power radiometer is the TPR.py code. This module adds a custom block to GRC that can then be called and used like any other block in GRC. A screenshot of the blocks used in this is shown below.

#### Total Power Radiometer Block

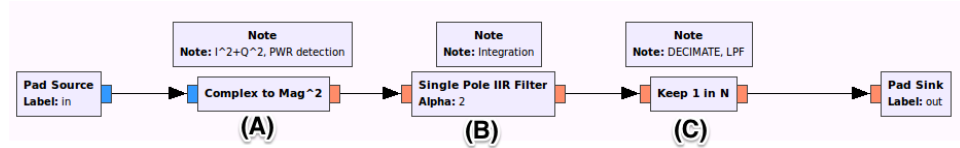


Figure A.1 Blocks used for creating a total power radiometer in software. Source: GNURadio Companion

```

#!/usr/bin/env python

#####
# Gnuradio Python Flow Graph
# Title: Total Power Radiometer
# Author: Matthew Nelson
# Description: Blocks for power detection, integration and LPF
# for a total power radiometer
# Generated: Sun Apr 12 23:03:59 2015
#####

from gnuradio import blocks
from gnuradio import filter
from gnuradio import gr
from gnuradio.filter import firdes

class TPR(gr.hier_block2):

    def __init__(self, integ=1, samp_rate=1, det_rate=1):
        gr.hier_block2.__init__(
            self, "Total Power Radiometer",
            gr.io_signature(1, 1, gr.sizeof_gr_complex*1),
            gr.io_signature(1, 1, gr.sizeof_float*1),
        )

```

```

#####
# Parameters

#####
self.integ = integ
self.samp_rate = samp_rate
self.det_rate = det_rate

#####

# Blocks

#####
self.single_pole_iir_filter_xx_0 = filter.
    single_pole_iir_filter_ff(1.0/((samp_rate*integ)/2.0) ,
    1)
(self.single_pole_iir_filter_xx_0).set_processor_affinity
([1])
self.blocks_keep_one_in_n_4 = blocks.keep_one_in_n(gr.
    sizeof_float*1, samp_rate/det_rate)
self.blocks_complex_to_mag_squared_1 = blocks.
    complex_to_mag_squared(1)

#####

# Connections

#####
self.connect((self.blocks_complex_to_mag_squared_1, 0), (
    self.single_pole_iir_filter_xx_0, 0))
self.connect((self.blocks_keep_one_in_n_4, 0), (self, 0))
self.connect((self, 0), (self.

```

```
    blocks_complex_to_mag_squared_1, 0))

self.connect((self.single_pole_iir_filter_xx_0, 0), (self
    .blocks_keep_one_in_n_4, 0))

def get_integ(self):
    return self.integ

def set_integ(self, integ):
    self.integ = integ
    self.single_pole_iir_filter_xx_0.set_taps(1.0/((self.
        samp_rate*self.integ)/2.0))

def get_samp_rate(self):
    return self.samp_rate

def set_samp_rate(self, samp_rate):
    self.samp_rate = samp_rate
    self.single_pole_iir_filter_xx_0.set_taps(1.0/((self.
        samp_rate*self.integ)/2.0))
    self.blocks_keep_one_in_n_4.set_n(self.samp_rate/self.
        det_rate)

def get_det_rate(self):
    return self.det_rate

def set_det_rate(self, det_rate):
    self.det_rate = det_rate
```

```
self.blocks_keep_one_in_n_4.set_n(self.samp_rate/self.  
det_rate)
```

## Python code for analyzing data

IPython notebooks was used to perform an analysis on the data. The code presented here is the export of this notebook. The Markdown language as well as some HTML is used to create easy to read pages that include the python code, generated graphs and descriptive text.

---

### Total Power Radiometer

```
#-*- coding: utf-8
#Radiometer Parsing Function

#This code shows an example of reading in and plotting data that
is outputted from a GNURadio GRC file.

#In this example a Total Power Radiometer is developed in
GNURadio GRC and uses the File Sink function to store the data
.

#The plot then shows the total power output from the radiometer
as a matched load is submerged in Liquid Nitrogen,
#then Ice Water and then left to dry.

# - - -
#
### Read the data

# Import Needed functions

# Import needed libraries
from pylab import *
import pylab
import scipy
```

```
import numpy
import scipy.io as sio
import csv

# Use this to set the filename for the data file and CSV
Calibration file.

tpr = 'tpr_2014.06.12.Lab0.dat'
calib = 'tpr_calib_2014.06.12.Lab0.csv'
x2_data = 'tpr_x2_2014.06.12.Lab0.csv'

# Uses SciPy to open the binary file from GNURadio

f = scipy.fromfile(open(tpr), dtype=scipy.float32)

# Because of the valve function in GNURadio, there are zeros that
get added to the file. We want to trim out those zeros.

# In [5]:

f = numpy.trim_zeros(f)
```

```

# Create an index array for plotting. Also, since we know the
interval the data is taken, we can convert this to an actual
time.

# In [6] :

y = numpy.linspace(0,(len(f)*.5),numpy.size(f))

#### Plot the data

# In [7] :

plot(y,f)
xlabel('Time (sec)')
ylabel('rQ Values')
title('rQ vs Time')
grid(True)

pylab.show()

# ## Calibration

# The rQ values are the raw values from the total power
radiometer and are uncalibrated. While the graph shows the
change in the total power recorded and shows that the
radiometer can detect changes in noise temperature, it has no
other meaning than that. What we want is to show what the

```

*total power is in relation to a noise temperature. Since we have recorded the values of the rQ at fixed and known teperatures, we can create a calibration line and calibrate the radiometer. For this experiment, we found that the following values matched our two known temperatures.*

```

#
# /rQ Value/X^2 Voltage/Temperature
# /-----/-----
# .0977    / 1.9617      /77 K
# .1507    / 2.085       /273.15 K
#
# We can now solve for y = mx + b since we have two equations and
# two unknowns.
#
# To work with this, a calibration file is created. This is a
# very simple CSV file that contains 3 values: The raw rQ value,
# the raw voltage from the square-law detector (discussed later
# ) and the observed temperature. The table above would then
# look like the following in the file.
#   ''
# .0977,1.9617,77
# .1507,2.085,273.15
#   ''
#   - - -
#
# We need to read in the values from our CSV file that contains
# the values
```

```
# In [67]:
```

```

read_csv = open(calib, 'rb')
csvread = csv.reader(read_csv)
rQ_values = []
temp_values = []
voltage = []

for row in csvread:
    rQ, volt, temp = row
    rQ_values.append(float(rQ))
    voltage.append(float(volt))
    temp_values.append(float(temp))
read_csv.close()

a = numpy.array([[rQ_values[0], 1.0], [rQ_values[1], 1.0]], numpy.
    float32)
b = numpy.array([temp_values[0], temp_values[1]])

z = numpy.linalg.solve(a, b)
print z

# Now we apply these values to the array that holds our raw rQ
# values

g = f*z[0]+z[1]

```

```

# Now we can re-plot the graph but this time with the calibrated
noise temperatures

plt.figure()
plot(y,g)
xlabel('Time')
ylabel('Noise Temperature (K)')
title('Temp vs Time')
grid(True)

pylab.show()

# This is looking better, but the time at the bottom doesn't have
much meaning. Since we know the sample rate of the Software
Defined Radio, we can calculate the time interval between each
sample.

# - - -
# # Square-law data
#
# We now want to look at the data from the Square-Law detector to
verify the operation of the SDR. In the experiment that was
conducted above, a power splitter was used to split the RF
signal so that one went to the SDR and the other to a square-
law detector (with a 3.1 dB loss though). Therefore both data
should be the same. Let's read and then plot this data.

```

```

read_csv = open(x2_data, 'rb')
csvread = csv.reader(read_csv)
dummy = []
x2_voltage = []

for row in csvread:
    dummy, x2voltage = row
    x2_voltage.append(float(x2voltage))
read_csv.close()

# Like the SDR data, we want to have a time reference at the bottom.

w = numpy.linspace(0,(len(x2_voltage)*.01),numpy.size(x2_voltage))
)

plt.figure()
plot(w,x2_voltage)
xlabel('Time (sec)')
ylabel('Voltage (V)')
title('X^2 Voltage vs Time (Noisy)')
grid(True)

pylab.show()

# The Square-law detector doesn't have a filter on it unlike the data we get from the SDR. The GNURadio program takes the data

```

*and applies a Low Pass Filter to "clean up" the information.  
We need to do the same with our Square-law data.*

```

from scipy import signal

N=100

Fc=2000

Fs=1600

h=scipy.signal.firwin(numtaps=N, cutoff=40, nyq=Fs/2)
x2_filt=scipy.signal.lfilter(h,1.0,x2_voltage)

plt.figure()
plot(w,x2_filt)
xlabel('Time (sec)')
ylabel('Voltage (V)')
title('X^2 Voltage vs Time')
axis([0, 610, 1.94, 2.12])
grid(True)

pylab.show()

# Now we wish to calibrate this data as well. We will use the  
same file and use the calibration points in that file.

a = numpy.array([[voltage[0],1.0],[voltage[1],1.0]],numpy.float32)
b = numpy.array([temp_values[0],temp_values[1]])

```

```
z = numpy.linalg.solve(a,b)
print z

x2_calib = x2_filt*z[0]+z[1]

plt.figure()
plot(w,x2_calib)
xlabel('Time (sec)')
ylabel('Voltage (V)')
title('X^2 Noise Temp vs Time')
axis([0, 610, 70, 300])
grid(True)

pylab.show()

# This looks to be the same as our SDR graph, but let's overlay
them to make sure

plt.figure()
plot(w,x2_calib,'r',label='X^2')
plot(y,g,'b',label='SDR')
xlabel('Time (sec)')
ylabel('Voltage (V)')
title('Noise Temperature vs Time')
axis([0, 610, 70, 300])
grid(True)
legend(loc='lower right')
```

```
# We have some timeshift due to two reasons. One, the timing isn't always perfect when starting the collection of the two data sets. And two, we get a timeshift from filtering the square-law data
```

```
pylab.show()
```

## BIBLIOGRAPHY

- Aitken, G. J. M. (1968). A new correlation radiometer. *Antennas and Propagation, IEEE Transactions on*, 16(2):224–228.
- Behnke, P., Soberal, D., Bredeweg, S., Dunne, B., Sterian, A., and Furton, D. (2013). Senior capstone: A software defined radio design for amateur astronomy. In *Interdisciplinary Engineering Design Education Conference (IEDEC), 2013 3rd*, pages 104–111.
- Bremer, J. C. (1979). Improvement of scanning radiometer performance by digital reference averaging. *Instrumentation and Measurement, IEEE Transactions on*, 28(1):46–54.
- Clapp, R. and Maxwell, J. (1967). Complex-correlation radiometer. *Antennas and Propagation, IEEE Transactions on*, 15(2):286–290.
- Cross, D. (1998). Time domain filtering techniques for digital audio. Website. <http://groovit.disjunkt.com/analog/time-domain/timfilt.html>.
- De Roo, R., Ruf, C., and Sabet, K. (2007). An l-band radio frequency interference (rfi) detection and mitigation testbed for microwave radiometry. In *Geoscience and Remote Sensing Symposium, 2007. IGARSS 2007. IEEE International*, pages 2718–2721.
- Dicke, R. H. (1946). The measurement of thermal radiation at microwave frequencies. *Review of Scientific Instruments*, 17(7):268–275.
- Ellingson, S., Hampson, G., and Johnson, J. (2003). Design of an l-band microwave radiometer with active mitigation of interference. In *Geoscience and Remote Sensing Symposium, 2003. IGARSS '03. Proceedings. 2003 IEEE International*, volume 3, pages 1751–1753.

- Erbas, C., Hornbuckle, B., and De Roo, R. (2006). Iowa state university/the university of michigan direct sampling digital radiometer. In *Geoscience and Remote Sensing Symposium, 2006. IGARSS 2006. IEEE International Conference on*, pages 3074–3077.
- Evans, G. and McLeish, C. W. (1977). *RF Radiometer Handbook*. Artech House, Dedham, MA.
- Fischman, M. A. (2001). *Development of a direct-sampling digital correlation radiometer for earth remote sensing applications*. PhD thesis, University of Michigan.
- Forte, G., Tarongi Bauza, J., dePau, V., Vall llossera, M., and Camps, A. (2013). Experimental study on the performance of rfi detection algorithms in microwave radiometry: Toward an optimum combined test. *Geoscience and Remote Sensing, IEEE Transactions on*, 51(10):4936–4944.
- Fujimoto, K. (1964). On the correlation radiometer technique. *Microwave Theory and Techniques, IEEE Transactions on*, 12(2):203–212.
- Hardy, W. N., Gray, K., and Love, A. (1974). An s-band radiometer design with high absolute precision. *Microwave Theory and Techniques, IEEE Transactions on*, 22(4):382–390.
- Jonard, F., Weihermuller, L., Jadoon, K., Schwank, M., Vereecken, H., and Lambot, S. (2011). Mapping field-scale soil moisture with l-band radiometer and ground-penetrating radar over bare soil. *Geoscience and Remote Sensing, IEEE Transactions on*, 49(8):2863–2875.
- Jondral, F. K. (2005). Software-defined radio: basics and evolution to cognitive radio. *EURASIP journal on wireless communications and networking*, 2005(3):275–283.
- Kerr, Y. (2012). Smos rfi detection: Today’s maps. Website. [http://www.cesbio.ups-tlse.fr/SMOS\\_blog/?p=2963](http://www.cesbio.ups-tlse.fr/SMOS_blog/?p=2963).
- Leech, M. (2006). Gnuradio and usrp: Solderless breadboarding for the 21st century. In *25th Anniversary Conference of the Society of Amateur Radio Astronomers*.

- Leech, M. and Ocame, D. (2007). A year of gnu radio and sdr astronomy: experience, practice and observations. Website. [http://www.sbrac.org/documents/gnuradio\\_at\\_one\\_year\\_20070401.doc](http://www.sbrac.org/documents/gnuradio_at_one_year_20070401.doc).
- Leinweber, G. (2001). Square law diode detectors in 50 ohm systems.
- Liu, P.-W., Judge, J., DeRoo, R., England, A., and Luke, A. (2013). Utilizing complementarity of active/passive microwave observations at l-band for soil moisture studies in sandy soils. In *Geoscience and Remote Sensing Symposium (IGARSS), 2013 IEEE International*, pages 743–746.
- McIntyre, E. and Gasiewski, A. (2012). A new technique for detecting the presence of weak interfering digital signals in radiometric noise. In *Geoscience and Remote Sensing Symposium (IGARSS), 2012 IEEE International*, pages 1517–1520.
- McIntyre, E. and Gasiewski, A. (2007). An ultra-lightweight l-band digital lobe-differencing correlation radiometer (ldcr) for airborne uav sss mapping. In *Geoscience and Remote Sensing Symposium, 2007. IGARSS 2007. IEEE International*, pages 1095–1097.
- McMullan, K. D., Brown, M., Martin-Neira, M., Rits, W., Ekholm, S., Marti, J., and Lemanczyk, J. (2008). Smos: The payload. *Geoscience and Remote Sensing, IEEE Transactions on*, 46(3):594–605.
- Misra, S., De Roo, R., and Ruf, C. (2012). An improved radio frequency interference model: Reevaluation of the kurtosis detection algorithm performance under central-limit conditions. *Geoscience and Remote Sensing, IEEE Transactions on*, 50(11):4565–4574.
- Mitola, J. (1995). The software radio architecture. *Communications Magazine, IEEE*, 33(5):26–38.
- Nyquist, H. (1928). Thermal agitation of electric charge in conductors. *Physical review*, 32(1):110–113.
- Ohm, E. and Snell, W. (1963). A radiometer for a space communications receiver. In *Antennas and Propagation Society International Symposium, 1963*, volume 1, pages 16–20.

- Rashid, R. A., Sarijari, M. A., Fisal, N., Yusof, S. K. S., and Mahalin, N. H. (2011). Spectrum sensing measurement using gnu radio and usrp software radio platform. In *ICWMC 2011: The Seventh International Conference on Wireless and Mobile Communications*, pages 237–242.
- Richaume, P. (2012). Outburst of anger. Website. [http://www.cesbio.ups-tlse.fr/SMOS\\_blog/?p=3381](http://www.cesbio.ups-tlse.fr/SMOS_blog/?p=3381).
- Ruf, C. and Gross, S. (2010). Digital radiometers for earth science. In *Microwave Symposium Digest (MTT), 2010 IEEE MTT-S International*, pages 828–831.
- Sarijari, M., Marwanto, A., Fisal, N., Yusof, S. K. S., Rashid, R., and Satria, M. (2009). Energy detection sensing based on gnu radio and usrp: An analysis study. In *Communications (MICC), 2009 IEEE 9th Malaysia International Conference on*, pages 338–342.
- Shi, J., Njoku, E., Chen, K., Jackson, T., and O’niell, P. (2003). Estimation of soil moisture with repeat-pass l-band radiometer measurements. In *Geoscience and Remote Sensing Symposium, 2003. IGARSS ’03. Proceedings. 2003 IEEE International*, volume 1, pages 413–415 vol.1.
- Skou, N. and Vine, D. L. (2006). *Microwave Radiometer Systems Design and Analysis*. Artech House, Norwood, MA.
- Tiuri, M. (1964). Radio astronomy receivers. *Antennas and Propagation, IEEE Transactions on*, 12(7):930–938.
- Ulaby, F. T. and Long, D. G. (2014). *Microwave Radar and Radiometric Remote Sensing*. The University of Michigan Press, Ann Arbor, MI.
- Ulaby, F. T., Moore, R. K., and Fung, A. K. (1981). *Microwave Remote Sensing*. Artech House, Dedham, MA.
- Villarino, R., Enrique, L., Camps, A., Corbella, I., and Blanch, S. (2002). Design, implementation and test of the upc l-band automatic radiometer. In *Proc. URSI Commission-F 2002 Open Symp.*

- Wang, Z., Liu, J., Lu, H., Zheng, W., Wang, X., and Li, B. (2012). A digital correlation full-polarimetric microwave radiometer design and calibration. In *Geoscience and Remote Sensing Symposium (IGARSS), 2012 IEEE International*, pages 4688–4690.
- Weng, Q. (2012). *An Introduction to Contemporary Remote Sensing*. McGraw-Hill's AccessEngineering. Mcgraw-hill.